

1      **An Overview of Antarctic Sea Ice in CESM2, Part I:**  
2      **Analysis of the Seasonal Cycle in the Context of Sea**  
3      **Ice Thermodynamics and Coupled**  
4      **Atmosphere-Ocean-Ice Processes**

5      **Hansi K.A. Singh<sup>1</sup>, Laura Landrum<sup>2</sup>, Marika M. Holland<sup>2</sup>, David A. Bailey<sup>2</sup>,**  
6      **and Alice K. DuVivier<sup>2</sup>**

7                   <sup>1</sup>School of Earth and Ocean Sciences, University of Victoria, Victoria BC Canada

8                   <sup>2</sup>Climate and Global Dynamics Laboratory, National Center for Atmospheric Research, Boulder CO USA

9      **Key Points:**

- 10     • Antarctic sea ice is thinner and less extensive in CESM2 than in CESM1.  
11     • A new mushy-layer thermodynamics formulation in CICE5 accelerates ice growth  
12       in coastal polynyas and augments snow-to-ice conversion.  
13     • Greater surface wind stress curl increases warm water upwelling under the ice pack  
14       in CESM2, which thins ice and decreases its extent.

15 **Abstract**

16 We assess Antarctic sea ice climatology and variability in CESM2, and compare it to that  
 17 in CESM1 and (where appropriate) real-world observations. In CESM2, Antarctic sea  
 18 ice is thinner and less extensive than in CESM1, though sea ice area (SIA) is still ap-  
 19 proximately 1 million km<sup>2</sup> greater in CESM2 than in present-day observations. Though  
 20 there is less Antarctic sea ice in CESM2, the annual cycle of ice growth and melt is more  
 21 vigorous in CESM2 than in CESM1. A new mushy-layer thermodynamics formulation  
 22 implemented in the latest version of CICE in CESM2 accounts for both greater frazil ice  
 23 formation in coastal polynyas and more snow-to-ice conversion near the edge of the ice  
 24 pack in the new model. Greater winter ice divergence in CESM2 (relative to CESM1)  
 25 is due to stronger stationary wave activity and greater wind stress curl over the ice pack.  
 26 Greater wind stress curl, in turn, drives more warm water upwelling under the ice pack,  
 27 thinning it and decreasing its extent. Overall, differences between Antarctic sea ice in  
 28 CESM2 and CESM1 arise due to both differences in their sea ice thermodynamics for-  
 29 mulations, and differences in the coupled atmosphere-ocean state.

30 **Plain Language Summary**

31 Sea ice is a central part of the Antarctic climate system, and Earth system mod-  
 32 els are an indispensable tool for studying the climate of the Antarctic. Advances in mod-  
 33 elling are essential for understanding and projecting future changes in the region as the  
 34 globe warms. Here, we describe Antarctic sea ice climatology in the state-of-the-art Com-  
 35 munity Earth System Model, version 2 (CESM2). CESM2 incorporates several modelling  
 36 advances which collectively improve representation of Antarctic climate compared to pre-  
 37 vious model versions. Among these is a 'mushy layer' treatment of sea ice, where the ice  
 38 is modelled as a mixture of solid ice and salty water. Modeling sea ice as a mushy layer  
 39 changes the way that Antarctic sea ice grows in CESM2, in a manner more closely re-  
 40 sembling how Antarctic sea ice has been observed to grow in the real world. Antarctic  
 41 sea ice area in CESM2 also more closely matches observed sea ice area, due primarily  
 42 to differences in atmospheric winds and ocean heating. In conjunction with observations  
 43 and other state-of-the-art global climate models, CESM2 will be an important tool for  
 44 furthering understanding of Antarctic climate at present and in the future.

45      **1 Introduction**

46      Sea ice is a fundamental, dynamic component of the Antarctic climate system. Antarctic  
 47      sea ice undergoes extraordinary expansion and retreat over the seasons: ice area ex-  
 48      pands from a mere 2 million km<sup>2</sup> at its end-of-summer minimum to nearly 15 million km<sup>2</sup>  
 49      at its spring maximum (Gordon, 1981; Parkinson & Cavalieri, 2012). This massive sea-  
 50      sonal growth and retreat of ice area impacts nearly every aspect of the Antarctic sys-  
 51      tem, from atmospheric stability and ocean dynamics, to ice sheet mass balance and bi-  
 52      ological productivity.

53      The presence of sea ice strongly attenuates (turbulent and radiative) heat and mo-  
 54      mentum conveyance between the atmosphere and ocean (Eicken, 2003), and the state  
 55      of the lower troposphere in the high latitudes, including cloudiness, boundary layer depth,  
 56      and stability, varies substantially with sea ice cover (see, e.g., Wall et al., 2017; Mor-  
 57      rison et al., 2018). Sea ice melt and growth impact ocean hydrography through fresh-  
 58      water capping and brine rejection, respectively (Pelichero et al., 2017); brine rejection  
 59      plays a crucial role in creating low-buoyancy shelf waters off the Antarctic coast that form  
 60      Antarctic Bottom Water, the coldest and densest water in the world oceans (Goosse et  
 61      al., 1997; Ohshima et al., 2013). Calving from marine ice shelves, which flow from the  
 62      Antarctic ice sheet, may be thwarted by the presence of sea ice cover or hastened by its  
 63      absence (Massom et al., 2018). The Southern Ocean food web, essential for global food  
 64      security, depends on the seasonal cycle of sea ice, with several keystone species relying  
 65      on sea ice cover over the course of their developmental cycles (Garrison & Buck, 1989).  
 66      The Antarctic climate system, both present and future, cannot be understood in full with-  
 67      out a reasonable reckoning of the sea ice and its seasonality.

68      Antarctic sea ice differs in many respects from Arctic sea ice. The magnitude of  
 69      the seasonal cycle over the Arctic is smaller than that over the Antarctic, with multi-  
 70      year ice dominating much of Arctic icepack volume historically. Antarctic sea ice is thin-  
 71      ner and more extensive (particularly in winter), while Arctic sea ice is thicker and more  
 72      contained in area (Rothrock et al., 1999; Worby et al., 2008), as the Arctic basin is nearly  
 73      landlocked by the North American and Eurasian continents. As Antarctic sea ice extends  
 74      further equatorward than Arctic sea ice, it is more exposed to fluctuations in the sur-  
 75      face westerly wind maximum, and its variability is closely tied to the Southern Annu-  
 76      lar Mode (SAM; Kwok & Comiso, 2002; Simpkins et al., 2012; Raphael & Hobbs, 2014;

77 Holland et al., 2017) and related Amundsen Sea Low (Holland et al., 2018). Mechanisms  
78 of ice growth and melt also differ between the two hemispheres. Much Antarctic sea ice  
79 growth occurs in polynyas off the coast, as downslope (katabatic) winds flow from the  
80 high-elevation ice sheet to open coastal waters, driving frazil ice formation (Maqueda et  
81 al., 2004; Tamura et al., 2008). Snow falling over the ice pack also thickens Antarctic ice  
82 more so than Arctic ice, as snow weight lowers the freeboard below the sea surface, ini-  
83 tiating snow-to-ice conversion (Eicken et al., 1995; Massom et al., 2001; Maksym & Markus,  
84 2008). In spring and summer, Antarctic sea ice melts from its base as it retreats to its  
85 end-of-summer minimum, while Arctic ice melts at both top and bottom faces nearly equally  
86 (Perovich et al., 2014). Such differences between the hemispheres indicate that Antarc-  
87 tic sea ice must be understood as a component in a unique coupled system, distinct from  
88 that of the Arctic.

89 Antarctic sea ice has also responded very differently to a warming climate than Arc-  
90 tic sea ice. While Arctic sea ice has retreated significantly in response to anthropogenic  
91 greenhouse gas forcing, Antarctic sea ice underwent a modest expansion from 1979 to  
92 2015. This paradoxical expansion of Antarctic sea ice area, occurring concurrently with  
93 increasing global mean surface temperatures and rapid retreat of Arctic sea ice, was ini-  
94 tially attributed to stratospheric ozone loss over the Antarctic (J. Turner et al., 2009),  
95 or to an increase in freshwater fluxes into the Southern Ocean (due to ice shelf melt, for  
96 example; see Bintanja et al., 2013). Later studies suggested that neither the Antarctic  
97 ozone hole and associated positive SAM trend (Sigmond & Fyfe, 2010; Bitz & Polvani,  
98 2012) nor observed changes in freshwater forcing (Swart & Fyfe, 2013; Pauling et al., 2016)  
99 were sufficient to explain Antarctic ice area expansion. Natural variability in sea ice area,  
100 either driven by variability in Southern Ocean temperatures (Singh et al., 2019), vari-  
101 ability in Southern Ocean deep convection (Zhang et al., 2019), or variability in the trop-  
102 ics (Meehl et al., 2016), appears to be the simplest explanation for Antarctic sea ice area  
103 expansion over the satellite era. While Arctic sea ice area has experienced fluctuations  
104 due to natural variability over the satellite era (Swart et al., 2015), natural variability  
105 may play a greater role in Antarctic sea ice evolution because the response to greenhouse  
106 gas forcing, both transient and equilibrium, is weaker in the Antarctic than the Arctic  
107 (Armour et al., 2016; Singh et al., 2018).

108 Changes in Antarctic sea ice impact not only the climate local to the Antarctic,  
109 but also climate elsewhere. Idealized atmospheric dynamical core experiments suggest

that lower tropospheric heating in the high latitudes, similar to that resulting from sea ice loss, tends to push the eddy-driven jet and storm-track equatorward (McGraw & Barnes, 2016). Experiments which isolate the global climate response to (projected) late 21st century Arctic sea ice loss indicate a range of far-reaching impacts, including equatorward jet shifts in both hemispheres, a northward shift in the Intertropical Convergence Zone, and greater extratropical precipitation in both hemispheres (in a fully-coupled model; see Deser et al., 2015; Blackport & Kushner, 2017; Smith et al., 2017). Similar experiments performed to isolate the global climate response to Antarctic sea ice loss suggest a similar slew of remote responses, albeit weaker than the response to Arctic sea ice loss (England et al., 2018).

Though the local and global climate impacts of Antarctic sea ice are substantial, the study of Antarctic sea ice is hampered by the difficulty of obtaining *in situ* observations from remote regions with extreme climatic conditions. As such, global climate models employing sophisticated sea ice components, in which ice evolution is treated both thermodynamically and dynamically, are indispensable tools for study of the Antarctic climate system and its future fate.

Here, we present the first of a two-part overview of Antarctic sea ice in a newly-developed, state-of-the-art global climate model, version 2 of the Community Earth System Model (CESM2; see Danabasoglu et al., 2019). In this study, we focus on seasonal Antarctic sea ice climatology in the CESM2, including the many processes that control ice growth, melt, thickness, and area. In an ensuing companion study, we consider sea ice persistence and predictability, particularly the extent to which the Southern Ocean impacts sea ice predictability in the Antarctic.

The sea ice model in CESM2 is CICE5 (Hunke et al., 2015; Bailey et al., 2020, submitted), which employs a mushy-layer thermodynamics scheme (Feltham et al., 2006; A. Turner & Hunke, 2015), supplanting the constant salinity scheme used in earlier versions of the model (Bitz & Lipscomb, 1999, hereafter BL99). Incorporating prognostic salinity has been shown to improve representation of sea ice growth, melt, the ice thickness distribution, and ocean-ice interactions in both hemispheres in models (Vancoppenolle et al., 2009; A. Turner & Hunke, 2015), making it a significant advance in sea ice modelling.

141 In our analysis, we compare and contrast Antarctic sea ice pre-industrial climatol-  
 142 ogy in CESM2 to that in the older CESM1 (and, briefly, present-day observations). We  
 143 first assess differences in sea ice area, extent, and thickness between CESM2 and CESM1.  
 144 We then consider differences in sea ice growth (§3.1) and melt (§3.2) over the course of  
 145 the seasonal cycle, and the processes by which ice growth and melt occur in CESM2 com-  
 146 pared to CESM1. We then proceed to attribute these differences in the sea ice seasonal  
 147 cycle to, in some respects, differences in their thermodynamics treatments, or, in other  
 148 respects, to differences in their coupled atmosphere and ocean counterparts (§3.3). We  
 149 conclude by discussing several promising future research directions in the coupled evo-  
 150 lution of Antarctic sea ice highlighted by our analysis (§4).

## 151 2 Methodology

152 The state-of-the-art version 2 of the Community Earth System Model (CESM2)  
 153 is described in detail in Danabasoglu et al. (2019). All model components have been up-  
 154 dated extensively, incorporating cutting-edge physics essential to accurate simulation of  
 155 the Earth system. The atmosphere component of CESM2, CAM6 (Bogenschutz et al.,  
 156 2018), incorporates several parameterization advances, including a new unified atmospheric  
 157 convection scheme (CLUBB; see Guo et al., 2015; Larson, 2017), updated cloud micro-  
 158 physics (Gettelman & Morrison, 2015; Gettelman et al., 2015), aerosol impacts on cloud  
 159 formation (i.e. the aerosol indirect effect; see Hoose et al., 2010; Wang et al., 2014; Shi  
 160 et al., 2015), and more sophisticated treatments of orographic drag (Scinocca & McFar-  
 161 lane, 2000; Beljaars et al., 2004). Other model components, including the land, ocean,  
 162 and coupler, have also been updated (Danabasoglu et al., 2019).

163 The new CICE5 is described in depth by Hunke et al. (2015) and Bailey et al. (2020,  
 164 submitted). The most significant advance in the new model is in the treatment of sea  
 165 ice as a mushy layer, an amalgam of solid ice interspersed with microscopic pockets of  
 166 brine (Feltham et al., 2006; A. Turner & Hunke, 2015). In this case, the enthalpy of the  
 167 ice,  $q$ , is a weighted average of the enthalpy of the ice,  $q_i$ , and the enthalpy of the brine,  
 168  $q_{br}$ :

$$q = (1 - \phi)q_i + \phi q_{br} , \quad (1)$$

169 where  $\phi$  is the fraction of the sea ice mush made up of liquid brine. The enthalpy of the  
 170 ice evolves according to

$$\frac{\partial q}{\partial t} = \frac{\partial}{\partial z} \left( K \frac{\partial T}{\partial z} \right) + w \frac{\partial q_{br}}{\partial z} + F , \quad (2)$$

171 where  $T$  is the temperature of the mush,  $K$  is the vertical conductivity,  $w$  is the Darcy  
 172 velocity of the brine (used for parameterizing rapid and slow modes of gravity-driven brine  
 173 drainage; see A. Turner et al., 2013), and  $F$  represents the external energy flux to the  
 174 ice (from atmosphere or ocean). The (bulk) salinity of the ice ( $S = \phi S_{br}$ ) is a prognos-  
 175 tic variable, and is computed as

$$\frac{\partial(\phi S_{br})}{\partial t} = w \frac{\partial S_{br}}{\partial z} + G , \quad (3)$$

176 where  $G$  is a sink term modeling slow drainage of brine from ice (see A. Turner et al.,  
 177 2013). Inclusion of prognostic salinity into ice thermodynamics requires modifications  
 178 in the calculation of the ice thermal conductivity, basal growth rate, frazil growth rate,  
 179 rate of snow-to-ice conversion, and melt pond flushing (see A. Turner & Hunke, 2015).  
 180 Compared to constant-salinity sea ice thermodynamics (see Bitz & Lipscomb, 1999), mushy  
 181 layer thermodynamics augments both frazil and snow-to-ice growth: ice growth over open  
 182 water occurs more readily with less heat loss to the atmosphere, as new ice is represented  
 183 as an amalgam of solid ice and brine; and conversion of snow to ice is greater, as the thick-  
 184 ness of the newly formed ice is reckoned to be that of the seawater-flooded snow, not com-  
 185 pacted snow (A. Turner & Hunke, 2015).

186 Antarctic sea ice seasonal climatology and variability in CESM2 are evaluated over  
 187 the final 600 years of a 1100-year preindustrial run, where the atmospheric CO<sub>2</sub> concen-  
 188 tration is fixed at 280 ppm and all other atmospheric constituents are held at preindus-  
 189 trial levels (see Danabasoglu et al., 2019). All model components are (nominally) at 1°  
 190 spatial resolution. Sea ice seasonal climatology and variability in CESM2 is compared  
 191 to that over years 1100 to 1700 of the CESM1 Large Ensemble preindustrial run (Kay  
 192 et al., 2015). In order to assess the impact of mushy layer thermodynamics on the Antarc-  
 193 tic ice pack in CESM2, we also make use of a 50-year pre-industrial simulation performed  
 194 with a version of CESM2 where CICE5 uses the older Bitz and Lipscomb (1999) con-  
 195 stant salinity sea ice thermodynamics scheme (as described in Bailey et al., 2020, sub-  
 196 mitted, referred to hereafter as CESM2-BL99); CESM2 and CESM2-BL99 configurations  
 197 are identical in all other respects.

198 It is not necessarily appropriate (or useful) to compare CESM2 and CESM1 pre-  
199 industrial control experiments directly with observations over the satellite era, as present-  
200 day sea ice conditions have been subject to a variety of modern-day forcings, including  
201 greenhouse gases and stratospheric ozone depletion over the South pole, which were not  
202 present in the pre-industrial climate. However, where reasonable, we compare Antarc-  
203 tic sea ice climatologies from CESM2 and CESM1 preindustrial experiments with ob-  
204 servations of Antarctic sea ice area from 1979 to 2018, collected through passive microwave  
205 satellite retrieval and processed through NASA Team and Bootstrap algorithms (Cavalieri  
206 et al., 1996, updated yearly, 1999; Comiso & Nishio, 2008).

### 207 3 Results

208 We begin by comparing the seasonal cycle in monthly mean Antarctic sea ice area  
209 in CESM2, CESM1, and satellite observations from 1979 to 2018 (Fig 1). Overall, both  
210 models agree on the phasing of the sea ice seasonal cycle, and closely follow that of the  
211 satellite era observations. In both models and in observations, Antarctic sea ice area is  
212 minimal in February and maximal in September (Fig 1a). The sea ice growth season ex-  
213 tends from March through August, while the melt season is from October through Jan-  
214 uary; sea ice growth and melt, however, do occur year-round regionally in both CESM2  
215 and CESM1, as we describe further below.

216 CESM2 has significantly less Antarctic sea ice area than CESM1 year-round: Septem-  
217 ber sea ice area is approximately 1.5 million km<sup>2</sup> lower in CESM2 (15.9 million km<sup>2</sup> in  
218 CESM2 compared to 17.4 million km<sup>2</sup> in CESM1), while February sea ice area is approx-  
219 imately 1.0 million km<sup>2</sup> lower (2.7 million km<sup>2</sup> in CESM2 versus 3.7 million km<sup>2</sup> in CESM1).  
220 Though CESM2 has considerably less sea ice area than CESM1, sea ice area observed  
221 over the satellite era (1979 to 2018) is still approximately a half a million to a million  
222 km<sup>2</sup> less than that in CESM2 in the annual mean (Fig 1a, compare blue and cyan lines  
223 and with solid black line; Antarctic sea ice area in the NASA Team-processed satellite  
224 observations are approximately 0.4 million km<sup>2</sup> less than that in CESM2 in the annual  
225 mean, while ice area in the Bootstrap-processed observations are approximately 1.0 mil-  
226 lion km<sup>2</sup> less than that in CESM2 in the annual mean). Greater sea ice area in CESM2  
227 relative to satellite era observations may either reflect systematic biases in CESM2, or  
228 reflect the very different forcings present over the late 20th and early 21st centuries, com-  
229 pared to those imposed in the CESM2 pre-industrial experiment. Indeed, historical CESM2

230 runs evince much closer agreement between modelled sea ice area and observations (DuVivier  
 231 et al., 2019, submitted). Comparison of historical runs of state-of-the-art models par-  
 232 ticipating in the sixth Climate Model Intercomparison Project (CMIP6) show that CESM2  
 233 is one of few in which both February and September sea ice extent are within range of  
 234 those observed over the satellite era (only 7 models out of 40 showed such agreement;  
 235 see Roach et al., 2020).

236 We compare interannual variability in the sea ice seasonal cycle between CESM2,  
 237 CESM1, and satellite-era observations by comparing their standard deviations in monthly  
 238 sea ice area (Fig 1b). In general, CESM2 has less variability in monthly sea ice area than  
 239 CESM1, particularly from April to November, encompassing the mid- to late- growth  
 240 season and early melt season (Fig 1b, compare solid and dotted black lines). We further  
 241 assess the variability in monthly mean sea ice area in the two models by computing the  
 242 monthly sea ice area standard deviation in the models using all contiguous 40-year seg-  
 243 ments sampled from each pre-industrial control experiment, and comparing the envelope  
 244 of these standard deviations (Fig 1b, dark grey and light grey shaded regions show the  
 245 standard deviation range in CESM2 and CESM1, respectively) to the monthly standard  
 246 deviations in sea ice area from the last 39 years of the observations (Fig 1b, solid blue  
 247 and cyan lines). Over much of the seasonal cycle, the monthly sea ice area standard de-  
 248 viation in the observations falls within (or nearly within) the range of that in both mod-  
 249 els. However, the variability in the observations substantially exceeds that in both mod-  
 250 els in the middle of the melt season (November and December; compare shaded grey re-  
 251 gions to blue line in Fig 1b), suggesting that both models may have too little interan-  
 252 nual variability in the hemispheric total sea ice area at this time of year.

253 In Figure 2, we compare sea ice area and extent between CESM2 and CESM1, fo-  
 254 cusing on the annual mean, summer (December, January, and February average; DJF),  
 255 and winter (June, July, and August average; JJA). Reduced sea ice area and extent in  
 256 CESM2, relative to CESM1, is evident over most sectors and seasons around the con-  
 257 tinent, particularly the Ross Sea, Weddell Sea, and southern Indian Ocean; only the Amundsen-  
 258 Bellinghausen sector shows slightly greater sea ice extent in CESM2 compared to CESM1,  
 259 especially in winter (JJA; compare Figs 2g and h, and difference in Fig 2i). In summer  
 260 (DJF), decreased sea ice area and extent in CESM2 is evident around the whole conti-  
 261 nent, as the sea ice edge retreats substantially further towards the Antarctic coast in CESM2  
 262 compared to CESM1 (compare Figs 2d and e, and difference in Fig 2f).

263 Differences between CESM2 and CESM1 are also evident in the interannual vari-  
 264 ability of the location of the ice edge (Fig 2, dashed red lines). In both CESM2 and CESM1,  
 265 interannual variability in the ice edge is greatest over the West Antarctic sectors, par-  
 266 ticularly the Weddell and Amundsen-Bellinghausen Seas in summer (Figs 2d and e) and  
 267 winter (Figs 2g and h). In summer, there is greater interannual variability in the loca-  
 268 tion of the sea ice edge over the Ross and Weddell sectors of the West Antarctic in CESM2,  
 269 relative to CESM1. At the same time, there is somewhat less interannual variability in  
 270 the location of the ice edge over East Antarctic sectors in the CESM1, relative to CESM2  
 271 (Figs 2d and e).

272 In addition to having reduced area and extent, Antarctic sea ice is also somewhat  
 273 thinner in CESM2 than CESM1 (Fig 3, colors): circumpolar annual mean sea ice thick-  
 274 ness is 0.76 m in CESM2, compared to 0.78 m in CESM1. Thinner sea ice in CESM2  
 275 may possibly bring modeled ice thickness closer to that in present-day observations, reck-  
 276 oned to be  $0.62 \pm 0.67$  m for level ice in the annual mean (from shipboard observations  
 277 collected in the Antarctic Sea ice Process and Climate, ASPeCt, dataset; see Worby et  
 278 al., 2008), though ice thickness for both models lies well within the uncertainty range  
 279 of these observations. Moreover, ice thickness differences between the models vary greatly  
 280 between regional sectors. Year-round, the icepack in CESM2 is significantly thinner in  
 281 the Ross and (coastal) Amundsen-Bellinghausen sectors, relative to CESM1 (red shad-  
 282 ing in Figs 3c, f, i), but somewhat thicker in the Weddell and East Antarctic (Indian and  
 283 West Pacific) sectors. Because sea ice is (on average) slightly thinner and significantly  
 284 less extensive in CESM2, there is less ice volume in CESM2 relative to CESM1 ( $13.8 \times$   
 285  $10^3$  km $^3$  in CESM2 compared to  $14.6 \times 10^3$  km $^3$  in CESM1).

286 We also note substantial regional heterogeneity in Antarctic sea ice thickness over  
 287 the course of the seasonal cycle, which also differs in some respects between the two mod-  
 288 els. In both models, sea ice is thinnest over the East Antarctic sectors year-round, and  
 289 thickest over the West Antarctic: ice is thickest in the Amundsen, Bellinghausen, and  
 290 Ross seas in CESM1 (Fig 3a), and in the Amundsen and western Weddell seas in CESM2  
 291 (Fig 3b). In CESM1, sea ice remains thick over the Amundsen-Bellinghausen sector in  
 292 summer (Fig 3e), and also thickens over the Ross and Weddell sectors in winter (Fig 3g).  
 293 In CESM2, on the other hand, ice remains thick over the Amundsen and eastern Wed-  
 294 dell Seas in summer (Fig 3e), and also thickens over the Bellinghausen, western Wed-  
 295 dell, and Ross Seas in winter (Fig 3h). Thick ice also hugs much of the Antarctic coast

296 in CESM2, even in summer (Fig 3e). These regions of thicker coastal sea ice (reminis-  
 297 cent of land-fast sea ice, though CICE5 does not have a land-fast sea ice parameteriza-  
 298 tion) are particularly evident over the East Antarctic in CESM2 in summer, but are no-  
 299 tably absent in CESM1 (compare Figs 3d and e, and difference in 3f).

300 Thinner sea ice in CESM2 also corresponds to warmer surface skin temperatures  
 301 over the ice pack (compare the 260K isotherm in Figs 3a and b; also note differences in  
 302 Fig 3c). In summer, surface skin temperatures over much of the ice pack are at least 1K  
 303 warmer in CESM2 relative to CESM1 (Fig 3f), and a substantial portion of the ice pack  
 304 in CESM2 reaches the melting temperature (between 271K and 273K, depending on the  
 305 brine concentration of the ice). In CESM2, the 270K isotherm follows the Antarctic coast  
 306 over nearly all sectors (except the Weddell; see Fig 3e); in CESM1, on the other hand,  
 307 the 270K isotherm is distant from the coast, particularly over West Antarctic sectors (Fig  
 308 3d), indicating that much of the ice pack over this region never reaches the melting tem-  
 309 perature at the surface. In winter, surface temperatures are also greater in CESM2 than  
 310 CESM1 (compare Figs 3g and h, and differences in 3i), which may occur because thin-  
 311 ner sea ice has a greater equilibrium radiative temperature at its top surface than thicker  
 312 ice, all other factors being equal (see Thorndike, 1992; Leppäranta, 1993). Moreover, global  
 313 mean surface temperatures are approximately 1.2K warmer in CESM2 than CESM1 year-  
 314 round, which may also partly account for warmer surface temperatures over sea ice in  
 315 CESM2.

316 The seasonal cycle of hemispheric total ice growth and melt also differs substan-  
 317 tially between CESM2 and CESM1. The sea ice model (CICE5 in CESM2 and CICE4  
 318 in CESM1) computes thermodynamic and dynamic changes in ice thickness in separate  
 319 modules; changes in ice volume due to individual thermodynamic growth (basal, frazil,  
 320 and snow-to-ice) and melt (top, basal, and lateral) processes are calculated separately  
 321 and archived by the model, and the sum of these respective growth and melt terms is  
 322 shown in Figure 4. In general, the rates of ice growth and melt are larger in CESM2 than  
 323 CESM1 (Fig 4, compare solid and dotted lines), indicating that the sea ice annual cy-  
 324 cle is more intense in CESM2 than CESM1. In both models, ice grows most rapidly dur-  
 325 ing the growth season (March through August) and melts most rapidly during the melt  
 326 season (October through January); however, ice growth also occurs during the melt sea-  
 327 son, and ice melt also occurs during the growth season, albeit at slower rates. The rate  
 328 of sea ice growth in CESM2 exceeds the rate of sea ice growth in CESM1 year-round by

329 up to 50%, with the largest differences between the two models occurring in the late growth  
 330 season and early melt season (August to November; Fig 4, compare indigo lines). The  
 331 rate of sea ice melt is also greater in CESM2 over the growth season and the early melt  
 332 season (April through November); however, the rate of ice melt in CESM1 exceeds that  
 333 in CESM2 in the late melt season (January and February; Fig 4, compare red lines), pos-  
 334 sibly because there is substantially more sea ice available to melt in CESM1 than in CESM2  
 335 at this point in time.

336 As described earlier in §2, the most significant difference between the sea ice for-  
 337 mulations in the CICE5 (in CESM2) versus the CICE4 (in CESM1) is the mushy-layer  
 338 thermodynamics in the former, which has supplanted the BL99 thermodynamics in the  
 339 latter. However, neither the thinner ice pack nor the less extensive sea ice area in CESM2,  
 340 compared to CESM1, is directly attributable to differences in sea ice thermodynamics;  
 341 comparative studies of both thermodynamic formulations employed in the same sea ice  
 342 model, with all other model components being identical, suggest that the mushy-layer  
 343 formulation tends to thicken sea ice and increase the extent of the ice pack (A. Turner  
 344 & Hunke, 2015; Bailey et al., 2020, submitted), which is opposite the differences we find  
 345 between CESM2 and CESM1. In the following sections, we further explore how differ-  
 346 ences in sea ice growth and melt, partly attributable to these different formulations of  
 347 sea ice thermodynamics, interact with different atmospheric and oceanic factors in these  
 348 two models to produce the distinct Antarctic sea ice climatologies reported here.

### 349 3.1 Sea Ice Growth

350 We now consider differences between sea ice growth in CESM2 versus CESM1 in  
 351 greater detail. The CICE model simulates three types of sea ice growth (Hunke & Lip-  
 352 scomb, 2008): frazil (open-water) growth, where sea ice forms over open water as ocean  
 353 mixed layer temperatures drop below the freezing point; basal (congelation) growth, where  
 354 sea ice growth at the bottom surface of the ice is driven by conductive fluxes through  
 355 the ice; and snow-to-ice growth, where snow is converted to ice when the weight of over-  
 356 lying snow depresses the top surface of the ice below the sea surface. Total sea ice growth,  
 357  $dh/dt_{growth}$ , is due to the sum of basal, frazil, and snow-to-ice growth components:

$$\left( \frac{dh}{dt} \right)_{growth} = \left( \frac{dh}{dt} \right)_{basal} + \left( \frac{dh}{dt} \right)_{frazil} + \left( \frac{dh}{dt} \right)_{snow}. \quad (4)$$

358       Figure 5 shows the relative contributions of frazil, basal, and snow-to-ice terms in  
 359 monthly mean sea ice growth in CESM2 and CESM1. While basal growth is weaker in  
 360 CESM2 than CESM1, frazil and snow-to-ice growth are more vigorous. Greater snow-  
 361 to-ice and frazil growth, and decreased basal growth, are also found when mushy-layer  
 362 thermodynamics replaces BL99 in CICE5 within the fully-coupled CESM2 (CESM2-BL99;  
 363 see Bailey et al., 2020, submitted, and §2), suggesting that differences between CESM2  
 364 and CESM1 in the relative contributions of these sea ice growth terms can be attributed,  
 365 at least in part, to their different thermodynamic formulations (mushy-layer in CESM2/CICE5  
 366 versus BL99 in CESM1/CICE4).

367       Indeed, the magnitude and seasonality of each of the sea ice growth terms in CESM2-  
 368 BL99 is very similar to corresponding terms in CESM1 (Fig S1; compare dash-dot lines  
 369 to respective dotted lines), not CESM2, suggesting that the relative prevalence of dif-  
 370 ferent ice growth modalities strongly depends on the sea ice thermodynamics formula-  
 371 tion. Furthermore, other relevant factors that may impact ice growth are similar between  
 372 CESM2 and CESM2-BL99, indicating that these factors cannot be responsible for dif-  
 373 fferences in growth. Sea ice thickness, for example, impacts snow-to-ice growth: thicker  
 374 ice requires a greater mass of snow to depress the ice surface below the freeboard and  
 375 initiate conversion of accumulated snow to ice. However, the Antarctic ice pack in CESM2  
 376 and CESM2-BL99 is of similar thickness (Fig S2), suggesting that this factor cannot ac-  
 377 count for greater snow-to-ice conversion. Similarly, snowfall over the ice pack is nearly  
 378 indistinguishable between CESM2 and CESM2-BL99 (Fig S3), suggesting that differ-  
 379 ences in snow accumulation over sea ice are also not responsible for differences in snow-  
 380 to-ice conversion rates between the two. Finally, the surface wind stress in CESM2 and  
 381 CESM2-BL99 is very similar (Fig S4), indicating that greater frazil ice growth in CESM2  
 382 is unlikely to be due to greater sea ice divergence. Taken together, these lines of evidence  
 383 indicate that it is the mushy layer thermodynamics formulation that augments frazil and  
 384 snow-to-ice growth in CESM2 relative to CESM1, not differences in ice thickness, snow-  
 385 fall over the ice pack, or surface wind stress. In other words, replacing BL99 thermody-  
 386 namics with mushy layer thermodynamics is sufficient to augment frazil and snow-to-  
 387 ice growth, and decrease basal growth, even as other characteristics of the ice pack (such  
 388 as thickness), snowfall over ice, and surface wind stress, remain unchanged.

389       We now examine each sea ice growth term in further detail. The frazil (open-water)  
 390 sea ice growth rate is approximately twice as large in CESM2 as in CESM1 (Fig 5, com-

pare solid and dotted teal lines), and the peak in frazil ice formation occurs slightly later in the growth season in CESM2 (April in CESM1 versus May in CESM2). Greater frazil growth is facilitated by mushy-layer thermodynamics, as a brine-ice slurry can be formed with less latent heat exchange, compared to that required when ice salinity is assumed constant (A. Turner & Hunke, 2015). The spatial distribution of frazil sea ice growth also differs between CESM2 and CESM1 (compare Figs 6a, d, g with Figs 7a, d, g). While frazil growth can occur within the ice pack itself, particularly early in the season when the sea ice fraction is lower (see Figs 6a, 7a), most frazil growth occurs near the Antarctic coast in both models. However, coastal frazil growth is at least two to four times more vigorous in CESM2 than CESM1 throughout the growth season, especially over West Antarctic sectors. Frazil growth in CESM2-BL99 more closely resembles that in CESM1, not CESM2, indicating that the introduction of the mushy layer thermodynamics formulation in CESM2 is sufficient to instigate vigorous open-water ice formation off the coast (compare Fig S5a, d, e with Figs 6a, d, e and 7a, d, e).

Greater coastal frazil growth in CESM2 is especially significant in light of *in situ* observations of Antarctic sea ice formation in winter, which document vigorous ice production of several meters per year within coastal polynyas around the Antarctic continent (Tamura et al., 2008, 2016). Such coastal latent heat polynyas are driven by katabatic (down-slope) winds off the Antarctic continent, which elicit large turbulent fluxes from the ocean mixed layer, and advect newly-formed sea ice away from the coast to expose more open water for further open-water sea ice growth (reviewed by Maqueda et al., 2004). While the spatial distribution of polynyas in CESM2 agrees well with those reported by Tamura et al. (2016), the CESM2 has notably weak polynya activity in the Ross sector and over the West Antarctic peninsula compared to the observations.

Furthermore, buoyancy loss in these coastal polynyas, through both surface heat loss and brine rejection from newly-formed sea ice, supports formation of Antarctic Bottom Water (AABW), the most dense water in the world ocean (Goosse et al., 1997; Ohshima et al., 2013). More vigorous frazil ice formation in coastal polynyas in CESM2 relative to CESM1 hints at differences in AABW formation between the two models. Preliminary analysis of ocean salinity under ice suggests that the vertical salinity gradient is significantly greater in CESM2 than CESM1 (see SI, Fig S6). Further exploration of such differences is warranted (but beyond the scope of the present study).

In both models, basal (congelation) growth is the largest contributor to sea ice thickening over much of the growth season. The basal growth rate is approximately 25% smaller in CESM2 than CESM1 throughout the growth season (Fig 5, compare solid and dotted turquoise lines), and the peak in basal growth is approximately one month later in CESM1 than CESM2 (June in CESM1 versus May in CESM2). The spatial distribution of basal growth is similar in both models: greatest near the Antarctic coast, particularly over the East Antarctic sectors, and smallest near the ice edge (Figs 6b, e, h and Figs 7b, e, h). Basal growth is comparable in magnitude between both models at the beginning of the growth season (compare Fig 6b with Fig 7b), but declines much more in the mid- and late- growth season in CESM2 than CESM1 (compare Figs 6e, h with Figs 7e, h). Less basal growth in CESM2 compared to CESM1 is likely attributable to their different sea ice thermodynamics formulations: CESM2-BL99 has a basal growth rate similar to CESM1, not CESM2 (see SI, Fig S1). As we show later in §3.3, decreased basal growth in CESM2 is also consistent with greater ocean heat convergence under the ice pack in this model, compared to CESM1.

As basal growth declines in the mid- to late- growth season in both models, snow-to-ice growth increases, peaking at the ice area maximum in September, and persisting through the early melt season (Fig 5, purple lines). Observations of sea ice growth in the Antarctic suggest that snow-to-ice growth is particularly important in this hemisphere (Jeffries et al., 2001; Maksym & Markus, 2008): the Antarctic ice pack is thinner than that of the Arctic, and snowfall is more plentiful because of the adjacent storm track, making snow-to-ice growth an important component of the sea ice budget (Eicken, 2003). Antarctic snow-to-ice growth is nearly twice as large in CESM2 relative to CESM1, and the greater ice growth rate in CESM2 in the mid- to late- growth season and early melt season is entirely attributable to this term (recall Fig 4a). Unlike basal and frazil growth, which occur at the coast and at the center of the ice pack, snow-to-ice growth occurs near the edge of the ice pack in both models (compare Figs 6c, f, i to Figs 7c, f, i).

Significantly greater snow-to-ice growth in CESM2 is due, at least in part, to mushy-layer thermodynamics: because the mushy-layer formulation allows prognostic salinity within the ice, seawater flooding of snow layers is permitted as the weight of snow depresses ice below the water line, and the resulting ice growth is assessed to be the full depth of the flooded snow (i.e. snow plus brine; see A. Turner & Hunke, 2015). In the BL99 formulation, on the other hand, snow-to-ice growth is weaker because it is assumed

456 that snow must be compressed to produce ice, thereby decreasing the thickness of ice  
 457 that can be formed from the same quantity of snow. Indeed, the magnitude and seasonality  
 458 of snow-to-ice growth in CESM2-BL99 resembles that in CESM1, not CESM2, suggesting  
 459 that mushy layer thermodynamics plays an important role in augmenting conversion of accumulated snow to ice.  
 460

461 Somewhat thinner ice in CESM2 may also permit greater snow-to-ice growth, as  
 462 less snow is required to depress the surface of the ice below the water line (recall Fig 3).  
 463 However, we note that the winter sea ice pack is only thinner over some Antarctic sectors  
 464 in CESM2 (recall Fig 3i), but snow-to-ice growth is greater over all sectors (compare  
 465 Figs 6c, f, i with Figs 7c, f, i), suggesting that thinner ice is not the primary factor  
 466 responsible for greater snow-to-ice growth in CESM2. Moreover, snow-to-ice growth  
 467 in CESM2-BL99 resembles that in CESM1, not CESM2 (recall Fig S1; also compare Figs  
 468 S5c, f, i with Figs 6c, f, i and 7c, f, i), even though ice thickness is very similar between  
 469 CESM2-BL99 and CESM2 (recall Fig S2), further indicating that differences in ice thickness  
 470 are not primarily responsible for differences in snow-to-ice conversion rates.

471 Additionally, as shown in Figure 8, greater snow-to-ice growth in CESM2 may also  
 472 occur because of greater snowfall year-round over the ice pack. While there is greater  
 473 snowfall equatorward of the ice edge in winter and spring in CESM1 (Fig 8, brown colors  
 474 north of the ice edge), there is greater snowfall poleward of the ice edge year-round  
 475 in CESM2 (green colors south of the ice edge; note that only differences in June and July  
 476 are statistically significant at  $p < 0.05$ ). The latter increase permits more snow accu-  
 477 mulation near the edge of the ice pack in CESM2, and this snow is more readily converted  
 478 to ice. Indeed, there is less snow depth over sea ice in CESM2 than CESM1 (not shown)  
 479 though snowfall is greater, indicating more ready snow-to-ice formation in the former  
 480 than in the latter.

### 481 ***3.1.1 Relationships Between Sea Ice Growth Processes***

482 We now consider relationships between frazil, basal, and snow-to-ice growth terms,  
 483 as evaluated from lead-lag correlations between the area-integrated monthly mean value  
 484 of each term with every other term (as shown in Fig 9). We find many similarities, but  
 485 also significant differences, between these relationships in CESM2 compared to CESM1,

486 suggesting that mechanisms driving interannual variability in sea ice growth (and, there-  
 487 fore, ice area, extent, and volume) likely differ between the two models.

488 We begin with the relationship between basal and frazil growth, which differs markedly  
 489 between the two models (compare Figs 9a and b). In CESM1, greater frazil growth over  
 490 the growth season (February through September) is strongly correlated with greater basal  
 491 growth over concurrent and subsequent months (Fig 9a, red region). Conditions that fa-  
 492 vor frazil growth (such as strong upward turbulent and net radiative fluxes from surface  
 493 to atmosphere) also favor basal growth, so the close correspondence between these two  
 494 growth terms at zero lead-lag (i.e. concurrently) is unsurprising. Furthermore, frazil growth  
 495 earlier in the season may be necessary for subsequent basal growth later in the season,  
 496 as frazil growth provides a ‘platform’ of thin ice on which basal growth can commence.  
 497 While these reasonable relationships between frazil and basal growth are clearly evident  
 498 in CESM1, they are nearly absent in CESM2 (compare Figs 9a and b). This may be due  
 499 to weak basal growth in CESM2, relative to CESM1, which disrupts these expected cor-  
 500 relations between frazil and basal growth terms. Further study of these growth relation-  
 501 ships in both models is warranted.

502 The relationships between basal and snow-to-ice growth are more qualitatively sim-  
 503 ilar between the two models, though some differences are evident (compare Figs 9c and  
 504 d). In both CESM2 and CESM1, vigorous basal growth early in the growth season leads  
 505 to vigorous snow-to-ice growth later in the season (red regions in Figs 9c and d). This may  
 506 occur because basal growth early in the growth season creates a base of ice on which snow  
 507 can accumulate, facilitating snow-to-ice conversion later in the growth season. This re-  
 508 lationship persists to the end of the growth season and the early melt season (through  
 509 November) in CESM1, but tapers away in the late growth season (through August) in  
 510 CESM2. While basal growth promotes subsequent snow-to-ice growth in both models,  
 511 vigorous snow-to-ice growth in the mid- and late- growth season tends to inhibit con-  
 512 current and subsequent basal growth in both models (Figs 9c and d, blue regions). Snow-  
 513 to-ice growth depends on snow cover, which insulates the top surface of the sea ice, thereby  
 514 stymieing basal growth by decreasing the conductive flux through the ice (Powell et al.,  
 515 2005). Furthermore, snow-to-ice growth will thicken the ice, which will also reduce the  
 516 conductive flux through the ice and slow basal growth (Maykut & Untersteiner, 1971;  
 517 Thorndike, 1992). Though the negative correlation between late-season snow-to-ice con-  
 518 version and subsequent basal growth is present in both models, the relationship tapers

519 away more rapidly in CESM2 than CESM1 (by September in CESM2, but persisting through  
 520 December in CESM1).

521 The relationships between frazil growth and snow-to-ice growth are also qualita-  
 522 tively similar between the two models (Figs 9e, f). In both, greater frazil ice formation  
 523 early in the growth season (February to April) tends to lead greater snow-to-ice growth  
 524 later in the season (red regions in Figs 9e, f), though the relationship wanes more rapidly  
 525 with lead time in CESM2 than CESM1. Later in the growth season, however, greater  
 526 frazil ice formation is linked to less concurrent snow-to-ice growth (blue regions near the  
 527 dashed grey line in Figs 9e, f). Significant frazil growth later in the growth season may  
 528 be an indicator of a sluggish growth season, implying a more limited base on which snow-  
 529 to-ice conversion can occur. This latter relationship is conjectural, and more exploration  
 530 of this point may be warranted.

### 531 3.2 Sea Ice Melt

532 While sea ice growth differs substantively between CESM2 and CESM1, sea ice melt  
 533 is more qualitatively similar (Fig 10). The CICE model simulates three types of sea ice  
 534 melt: basal (occurring at the bottom of the ice), lateral (occurring on the lateral edge  
 535 of the ice), and top (occurring at the top face of the ice). Melt is greatest during the melt  
 536 season, but substantial melt also occurs during the growth season (recall Fig 4). In both  
 537 models, more than 95% of melt year-round occurs through basal melt (Fig 10, red lines),  
 538 with much smaller contributions from lateral and top melt during the mid- to late- melt  
 539 season (November through February; purple and gold lines in Fig 10). This distribution  
 540 of terms differs substantially from the melt budget in the Arctic, where top melt plays  
 541 a much larger role (Andreas & Ackley, 1982).

542 In CESM2, basal melt is greater than that in CESM1 over much of the year, in-  
 543 cluding over the growth season and the early melt season (March through November).  
 544 Greater basal melt in CESM2 is consistent with mushy-layer thermodynamics in this model,  
 545 as the melt pond flushing and gravity drainage formulations promote more vigorous basal  
 546 melt (A. Turner & Hunke, 2015; Bailey et al., 2020, submitted). However, basal melt in  
 547 CESM1 exceeds that in CESM2 in the mid- to late- melt season (January and Febru-  
 548 ary), which may occur because there is significantly more ice remaining to melt in CESM1  
 549 than CESM2 at this point in time.

550            **3.3 Sea Ice Dynamics and Thermodynamics**

551            We now consider the interplay between the thermodynamics of ice growth and melt,  
 552            described in the previous sections, and coupling between the sea ice, atmosphere, and  
 553            ocean. We begin by assessing the spatial pattern of changes in sea ice volume with time  
 554            (i.e. the ice volume tendency), which is due to the sum of thermodynamic and dynamic  
 555            terms:

$$\frac{dV}{dt} = \left( \frac{dV}{dt} \right)_{thermodynamics} + \left( \frac{dV}{dt} \right)_{dynamics}, \quad (5)$$

556            where the thermodynamic contribution to ice volume change,  $dV/dt_{thermodynamics}$ , is due  
 557            to the growth (frazil, basal, and snow-to-ice) and melt (basal, lateral, and top) processes  
 558            described previously; and the dynamic contribution,  $dV/dt_{dynamics} = -\nabla \cdot (\vec{v} V)$ , is  
 559            due to advection and convergence by the local ice pack velocity  $\vec{v}$  (Hunke & Lipscomb,  
 560            2008).

561            In Figure 11, we show the thermodynamic and dynamic contributions to the ice  
 562            volume tendency in CESM2 and CESM1 over selected months spanning the seasonal cy-  
 563            cle, highlighting the melt season (November and January) and the growth season (April  
 564            and July). Overall, both models generally agree qualitatively regarding these thermo-  
 565            dynamic and dynamic contributions to ice volume change, though important differences  
 566            do exist, as we describe further below. Over the melt season (November and January;  
 567            Figs 11a-d and 11e-h), there is a thermodynamic decrease in sea ice volume near the cen-  
 568            ter and edge of the ice pack in both models (red regions in Fig 11a, b, e, f), driven pri-  
 569            marily through basal melt (recall Fig 10). At the same time, there is a modest dynamic  
 570            divergence of ice volume away from the coast (red regions in Figs 11c, d), and a mod-  
 571            est dynamic convergence of ice volume near the ice edge (light blue regions near the black  
 572            ice edge contour in Figs 11c, d). Dynamic divergence of ice away from the center of the  
 573            ice pack during the melt season is slightly greater in CESM2 than CESM1 (compare Figs  
 574            11c and d), which may be a factor in promoting greater ice melt in this model, as ice melt  
 575            occurs more readily near the edge of the ice pack than at the center.

576            Over the growth season (April and July; Figs 11i-l and 11m-p), ice volume increases  
 577            through thermodynamic processes in both models (i.e. frazil, basal, and snow-to-ice growth,  
 578            as described in §3.1; blue regions in Figs 11i, j, m, n), but also declines through melt at  
 579            the ice edge (red regions near the black ice edge contour). At the same time, there is sig-  
 580            nificant dynamic divergence of ice volume away from the coast and center of the ice pack

581 in both CESM2 and CESM1 (red regions in Figs 11k, l, o, p), and dynamic convergence  
 582 of ice towards the edge of the ice pack (blue regions near the black ice edge contour). Thus,  
 583 over the course of the growth season, ice grows near the coast and the center of the ice  
 584 pack, diverges away from these regions of growth, converges towards the edge of the ice  
 585 pack, and melts at the ice edge.

586 Figure 12 highlights differences between CESM2 and CESM1 in the relative con-  
 587 tributions of thermodynamic and dynamic processes to the ice volume tendency over se-  
 588 lected months spanning the growth season (April, June, and August; shown as the dif-  
 589 ference between CESM2 and CESM1). First, we examine differences in the thermody-  
 590 namic contributions to the ice volume tendency between CESM2 and CESM1 (Figs 12a,  
 591 c, e). Over the course of the growth season, melt at the ice edge is significantly greater  
 592 in CESM2 than CESM1 (red regions near the black ice edge contours). Greater melt at  
 593 the ice edge in CESM2 is evident nearly everywhere, including the Weddell and Ross sec-  
 594 tors of the West Antarctic, and much of the East Antarctic. The Amundsen-Bellinghausen  
 595 sector is one of the only regions where melt at the ice edge is not significantly greater  
 596 in CESM2 than CESM1, though greater melt even here is evident near the end of the  
 597 growth season (August; Fig 12e).

598 There are also differences in the dynamic contribution to ice volume change between  
 599 CESM2 and CESM1 (Figs 12b, d, f). First, there is greater dynamic divergence of sea  
 600 ice away from the coast and the center of the ice pack in CESM2 throughout the growth  
 601 season (red regions in Figs 12b, d, f). Greater ice divergence is evident around much of  
 602 the continent, and is particularly pronounced over the East Antarctic sectors, the Wed-  
 603 dell Sea, and the Amundsen-Bellinghausen Seas. Greater transport of sea ice away from  
 604 the Antarctic coast in CESM2 may contribute to more vigorous frazil ice growth in coastal  
 605 polynyas in this model (recall Figs 5, 6, and 7). At the same time that more ice diverges  
 606 away from the Antarctic coast in CESM2, there is correspondingly greater dynamic con-  
 607 vergence of sea ice towards the ice edge (blue regions near the black ice edge contours).  
 608 Dynamic ice volume convergence near the ice edge in CESM2 is pronounced around nearly  
 609 the entire continent over the course of the growth season, though it is weakest relative  
 610 to CESM1 circa the Ross sector.

611 To better understand the mechanisms responsible for these differences in the ice  
 612 volume tendency between CESM2 and CESM1, we first examine the sea level pressure

in both models in Figure 13 (colors; shown for selected months spanning the growth season: April, June, and August). Both CESM2 and CESM1 exhibit a distinct tripole of low sea level pressure centers circling the Antarctic continent (as has been analyzed previously by Raphael, 2004, 2007): over the Amundsen-Bellinghausen sector, the south Indian sector, and the western south Pacific sector. These low pressure centers are significantly deeper in CESM2 than CESM1 (compare Figs 13b, d, f with 13a, c, e), indicating greater stationary wave activity in the former than the latter (Raphael, 2004). As a result, there is greater advection of sea ice by the cyclonic quasi-geostrophic near-surface flows that arise from these low pressure centers in CESM2 compared to CESM1 (compare arrows in Figs 13b, d, f with 13a, c, e; also see Raphael, 2007). Consequently, more sea ice is transported away from the center of the ice pack and towards its edges in CESM2, as suggested earlier by differences in the dynamic ice volume tendency in the two models (recall Fig 12).

Much stronger near-surface zonal winds accompany the stronger stationary wave activity in CESM2, as shown in Figure 14. Both surface easterlies and westerlies are stronger year-round in CESM2 relative to CESM1 (colors in Fig 14; near-surface zonal winds in CESM2 and CESM1 are shown by the blue solid and blue dotted contours, respectively), indicating greater surface wind stress in CESM2 than CESM1. Despite substantially stronger zonal winds in CESM2, the latitude of zero wind velocity (i.e. where easterlies transition to westerlies) is only slightly more equatorward in CESM2 than CESM1 (compare zero solid and dotted contours in Fig 14). As the meridional gradient in the zonal wind is greater in CESM2 than CESM1, there is greater wind stress curl over the ice pack and the Southern Ocean in the former than the latter.

Greater wind stress curl in CESM2 also implies greater wind-driven upwelling beneath the ice pack in this model, relative to CESM1. As waters at greater depth are warmer than near-surface waters at this latitude, greater upwelling results in greater heating by increased vertical advection (Fig 15, colors show the difference in heating by vertical motions between CESM2 and CESM1 in K/day). Greater heating by vertical upwelling in CESM2 is most evident directly below the mixed layer under the seasonal ice pack (i.e., between the minima and maxima of ice extent, delineated by the vertical turquoise lines, and below the green lines denoting the base of the mixed layer), and tends to decrease the stratification of the water column; as a consequence, the vertical distance between the 27.3 and 27.7 isopycnal contours is approximately 50m greater circa 65S in CESM2

than CESM1 (compare solid purple and dotted purple lines in Fig 15). Indeed, weaker stratification in CESM2 cannot be due to weaker buoyancy forcing by the sea ice seasonal cycle, as ice growth and melt in the CESM2 exceeds that in the CESM1 year-round (recall Fig 4). Greater heating by vertical advection is also evident in the mixed layer itself, circa 60S, which corresponds to the location of the mean ice edge near the middle and end of the ice growth season.

Stronger surface wind stress, greater wind stress curl, more heating by vertical advection, and weaker ocean stratification all contribute to greater ocean heat flux convergence in CESM2, relative to CESM1, as shown in Figure 16. The monthly ocean heat flux convergence in the mixed layer,  $Q$ , is calculated for both models as a residual from the month-to-month temperature tendency of the mixed layer,  $dT/dt$ , and the total surface heat flux,  $F_{sfc}$  (which includes ice-ocean heat exchange):

$$\rho_W c_p H_{ML} \frac{dT}{dt} = Q + F_{sfc}, \quad (6)$$

where  $\rho_W$  is the density of seawater,  $c_p$  is its heat capacity, and  $H_{ML}$  is the mixed layer depth (see Bitz et al., 2012).

Compared to CESM1, we find that the ocean heat flux convergence over the growth season is modestly greater under the ice pack and significantly greater at the ice edge in CESM2. Early in the growth season, there is significantly greater ocean heat flux convergence under the ice pack in CESM2 (April; Fig 16a), which persists to some extent over the course of the growth season (June through August; Figs 16b, c), and may limit basal growth (recall Fig 5) and sea ice thickness (recall Fig 3) in this model. In the mid- to late- growth season, greater ocean flux convergence is most evident at the ice edge in CESM2 (June and August; Figs 16b, c), and is responsible for greater melt here (recall the more negative thermodynamic ice volume tendency at the ice edge in CESM2 during the growth season, as shown in Figs 12a, c, e). Significantly, greater ocean heat flux convergence at the ice edge in CESM2 coincides with areas where the ice edge is more poleward in CESM2 relative to CESM1; this is particularly evident in the eastern Weddell, Indian, and the Ross sectors, and suggests that greater ocean heating may play an important role in limiting sea ice extent in these regions in CESM2. As greater wind stress and more intense stationary wave activity in CESM2 diverges ice away from the Antarctic coast and center of the ice pack, greater ocean heat flux convergence simultaneously limits ice thickness and extent.

**677 4 Discussion**

678 In this overview of Antarctic sea ice in the new CESM2, we describe its seasonal  
679 cycle, modalities of growth and melt, and interactions with both atmosphere and ocean,  
680 relative to that in CESM1. Overall, we find substantial differences between the old and  
681 new models, some of which are attributable to differences in how sea ice thermodynam-  
682 ics is treated, and others that are due to differences in the climatologies of the atmosphere  
683 and ocean.

684 Treating sea ice as a mushy layer, an amalgam with varying amounts of solid ice  
685 and microscopic liquid brine inclusions, rather than as a solid with fixed salinity (as in  
686 BL99), has been shown to impact the seasonal cycle of sea ice in both hemispheres (A. Turner  
687 & Hunke, 2015; Bailey et al., 2020, submitted). We find that in CESM2, the new mushy-  
688 layer thermodynamics treatment changes the spatial and temporal distribution of the  
689 different modalities of Antarctic sea ice growth relative to CESM1. Both frazil (open wa-  
690 ter) ice formation and snow-to-ice conversion make substantially greater contributions  
691 to Antarctic ice growth in CESM2 than CESM1, while basal (congelation) growth makes  
692 a smaller contribution. Greater frazil ice growth in CESM2 is concentrated within Antarc-  
693 tic coastal polynyas, while greater snow-to-ice conversion occurs at the center and edge  
694 of the growing ice pack. Observational studies show that such frazil and snow-to-ice growth  
695 processes are crucial for Antarctic sea ice growth in the real world (see, e.g., Jeffries et  
696 al., 2001; Maqueda et al., 2004; Maksym & Markus, 2008; Tamura et al., 2008, 2016),  
697 and it is possible that improved representation of these processes in the new model im-  
698 plies better agreement with real-world observations. Further quantitative intercompar-  
699 ison between model results (particularly historical, rather than pre-industrial, experi-  
700 ments) and present-day *in situ* observations is needed.

701 While differing sea ice growth in CESM2 and CESM1 is attributable in part to the  
702 differing sea ice thermodynamic treatments in the two models, differing sea ice thickness  
703 and extent are more clearly linked to differing atmosphere and ocean dynamics. The ex-  
704 tratropical atmospheric circulation in the Southern Hemisphere is more vigorous in CESM2  
705 than CESM1, with more energetic stationary wave activity and surface winds. Deeper  
706 subpolar low pressure centers in CESM2 sweep sea ice away from the coast (helping fa-  
707 cilitate frazil ice growth in coastal polynyas), increase sea ice divergence from the cen-  
708 ter of the ice pack, and drive sea ice equatorward. The latter tends to thin the ice pack,

which is evident in the climatology of Antarctic sea ice in CESM2. On the other hand, sea ice area and extent are substantially lower in CESM2 than CESM1 as ocean heat flux convergence into the mixed layer is greater in the new model. Greater surface wind stress curl in CESM2 is responsible for more upwelling of warmer waters from depth, increasing ocean heating under and at the edge of the ice pack; previous studies have shown that such increased ocean heat flux convergence acts as a substantial control on ice extent in Earth system models (Bitz et al., 2005). Were it not for this greater ocean heat input at the edge of the ice pack, it is likely that Antarctic sea ice area would be more extensive in CESM2 than it is.

Our study highlights the need to consider a range of inter-related factors when comparing sea ice in global climate models with each other and with real-world observations. It is possible for two models to have similar sea ice area and volume, but to have a very different confluence of processes that maintain this climatology: an ice pack maintained by high wind stress and copious snowfall may appear very similar in volume and area to one maintained by cold temperatures and substantial basal growth, for example. The prevalent modes of sea ice growth and melt, the relationships between these modes, and the magnitude of the seasonal cycle are likely all of import in maintaining climatological ice area and volume. Similarly, winds, ocean hydrography, and heating (by both atmospheric and oceanic processes) also impact the ice pack. We suggest that it may be useful for model intercomparisons to consider more of these auxiliary factors when evaluating how well global climate models simulate sea ice. We also suggest that some of these auxiliary factors, if observable in the real world, could serve to constrain models in a more comprehensive manner beyond ice area and thickness.

These other climatological factors may also impact how Antarctic sea ice responds to increased atmospheric CO<sub>2</sub> and other climate forcing agents. Traditionally, the sensitivity of the ice pack to climate warming has often been described in terms of ice area and thickness, with thicker and more extensive sea ice shown to experience greater decline as the globe warms (see, for example, Holland & Bitz, 2003; Bitz & Roe, 2004). However, other factors may also be equally important, including modes of ice growth, the strength of stationary waves and zonal winds over the ice pack, and the intensity of the seasonal cycle. A decline in ice volume, for example, may occur because ice growth slows, but different modes of ice growth may not be equally sensitive to climate warming: basal growth may decline as warmer ocean waters and less heat loss from the ice top hinder efficient

742 conduction through ice, but snow-to-ice conversion may increase if there is greater snow-  
 743 fall over the ice pack as the storm track shifts poleward. An ice pack that relies primarily  
 744 on basal growth may be more sensitive to warming temperatures than one that re-  
 745 lies more heavily on other modes of growth. As such, the relative sensitivity of the ice  
 746 pack to warming may depend on climatological factors beyond ice area and volume. We  
 747 suggest that consideration of such auxiliary factors may prove useful to further under-  
 748 standing of the mechanisms controlling the sensitivity of Antarctic sea ice to anthropogenic  
 749 forcing.

750 In this overview of Antarctic sea ice in the state-of-the-art CESM2, we have high-  
 751 lighted key differences in sea ice climatology and variability between the older CESM1  
 752 and the newer model. As Antarctic sea ice begins to retreat in response to a warming  
 753 climate, Earth system models will continue to be an important tool for understanding  
 754 the changing interplay between sea ice, ocean, and atmosphere in a warming world. CESM2,  
 755 in conjunction with observations, reanalyses, and other Earth system models, will serve  
 756 as an indispensable resource for understanding and anticipating these changes in Antarc-  
 757 tic climate in the future.

## 758 5 Concluding Points

759 The major findings of this study can be summarized as follows:

- 760 • Antarctic sea ice is less extensive and slightly thinner in CESM2 compared to CESM1.  
 761     Antarctic sea ice area in CESM2 more closely follows that in the satellite era ob-  
 762     servations, particularly in terms of maximum and minimum area.
- 763 • The seasonal cycle of Antarctic sea ice growth and melt are more intense in CESM2  
 764     than in CESM1.
- 765 • Mechanisms of sea ice growth in CESM2 differ substantially from those in CESM1:  
 766     frazil and snow-to-ice growth are greater, and basal growth is weaker.
- 767 • Differences in sea ice growth between CESM2 and CESM1 are primarily due to  
 768     the different sea ice thermodynamics schemes. Mushy layer thermodynamics, which  
 769     models prognostic salinity in the sea ice, increases snow-to-ice conversion and aug-  
 770     ments frazil (open-water) sea ice growth.

- Relationships between sea ice growth terms differ substantially between CESM2 and CESM1. Relationships are generally weaker in CESM2 than CESM1, particularly the link between early season frazil growth and later basal growth.
- During the growth season, there is greater stationary wave activity and greater westerly wind stress over the ice pack in CESM2, compared to CESM1. Stronger winds in CESM2 drive greater divergence of Antarctic sea ice away from the coast and center of the ice pack, and towards its edge.
- Greater wind stress curl over the ice pack in CESM2, relative to CESM1, drives more warm water upwelling. The resulting ocean heat flux convergence beneath the ice pack thins Antarctic sea ice in CESM2 and limits its extent.

### Acknowledgments

CESM2 model output used in this study is available at the NCAR Digital Asset Services Hub (DASH; <https://data.ucar.edu>) as casename *b.e21.B1850.f09\_g17.CMIP6-piControl.001*; CESM1 model output is available at the CESM Large Ensemble Community Project site (<http://www.cesm.ucar.edu/projects/community-projects/LENS/>) as casename *b.e11.B1850C5CN.f09\_g16.005*. The CESM project is supported primarily by the National Science Foundation (NSF). This material is based upon work supported by the National Center for Atmospheric Research (NCAR), which is a major facility sponsored by the NSF under Cooperative Agreement No. 1852977. Computing and data storage resources, including the Cheyenne supercomputer (doi:10.5065/D6RX99HX), were provided by the Computational and Information Systems Laboratory (CISL) at NCAR. LL was funded by NSF grant 1643484.

### References

- Andreas, E., & Ackley, S. (1982). On the differences in ablation seasons of Arctic and Antarctic sea ice. *Journal of the Atmospheric Sciences*, *39*(2), 440–447.
- Armour, K., Marshall, J., Scott, J., Donohoe, A., & Newsom, E. (2016, Jul). Southern Ocean warming delayed by circumpolar upwelling and equatorward transport. *Nature Geoscience*, *9*, 549-554.
- Bailey, D., Holland, M., DuVivier, A., Hunke, E., & Turner, A. (2020, submitted). Impact of sea ice thermodynamics in the CESM2 sea ice component. *Journal of Advances in Modeling Earth Systems*.
- Beljaars, A., Brown, A., & Wood, N. (2004). A new parametrization of turbulent

- 802 orographic form drag. *Quarterly Journal of the Royal Meteorological Society*,  
803 *130*(599), 1327–1347.
- 804 Bintanja, R., van Oldenborgh, G., Drijfhout, S. S., Wouters, B., & Katsman, C.  
805 (2013, Jul). Important role for ocean warming and increased ice-shelf melt in  
806 Antarctic sea ice expansion. *Nature Geoscience*, *6*, 376–379.
- 807 Bitz, C., Holland, M., Hunke, E., & Moritz, R. (2005, Aug). Maintenance of the sea  
808 ice edge. *Journal of Climate*, *18*, 2903–2921.
- 809 Bitz, C., & Lipscomb, W. (1999). An energy-conserving thermodynamic model of  
810 sea ice. *Journal of Geophysical Research: Oceans*, *104*(C7), 15669–15677.
- 811 Bitz, C., & Polvani, L. (2012). Antarctic climate response to stratospheric ozone de-  
812 pleation in a fine resolution ocean climate model. *Geophysical Research Letters*,  
813 *39*(L20705).
- 814 Bitz, C., & Roe, G. (2004). A mechanism for the high rate of sea ice thinning in the  
815 Arctic Ocean. *Journal of Climate*, *17*(18), 3623–3632.
- 816 Bitz, C., Shell, K., Gent, P., Bailey, D., Danabasoglu, G., Armour, K., … Kiehl, J.  
817 (2012). Climate sensitivity in the Community Climate System Model, version  
818 4. *Journal of Climate*, *25*(9), 3053–70.
- 819 Blackport, R., & Kushner, P. (2017). Isolating the atmospheric circulation response  
820 to Arctic sea ice loss in the coupled climate system. *Journal of Climate*, *30*(6),  
821 2163–2185.
- 822 Bogenschutz, P., Gettelman, A., Hannay, C., Larson, V., Neale, R., Craig, C., &  
823 Chen, C.-C. (2018). The path to CAM6: Coupled simulations with CAM5.4  
824 and CAM5.5. *Geoscientific Model Development (Online)*, *11*(LLNL-JRNL-  
825 731418).
- 826 Cavalieri, D., Parkinson, C., Gloersen, P., Comiso, J., & Zwally, H. (1999). De-  
827 riving long-term time series of sea ice cover from satellite passive-microwave  
828 multisensor data sets. *Journal of Geophysical Research: Oceans*, *104*(C7),  
829 15803–15814.
- 830 Cavalieri, D., Parkinson, C., Gloersen, P., & Zwally, H. (1996, updated yearly).  
831 *Sea ice concentrations from Nimbus-7 SMMR and DMSP SSM/I-SSMIS pas-*  
832 *sive microwave data, version 1.* NASA National Snow and Ice Data Center  
833 Distributed Archive Center.
- 834 Comiso, J., & Nishio, F. (2008). Trends in the sea ice cover using enhanced and

- 835 compatible AMSR-E, SSM/I, and SMMR data. *Journal of Geophysical Re-*  
836 *search: Oceans*, 113(C2).
- 837 Danabasoglu, G., Bates, S. C., Briegleb, B. P., Jayne, S. R., Jochum, M., Large,  
838 W. G., ... Yeager, S. G. (2012). The CCSM4 ocean component. *Journal of*  
839 *Climate*, 25(5), 1361–1389.
- 840 Danabasoglu, G., Lamarque, J.-F., Bacmeister, J., Bailey, D., DuVivier, A., Ed-  
841 wards, J., ... others (2019). The Community Earth System Model version 2  
842 (cesm2). *Journal of Advances in Modeling Earth Systems*.
- 843 Deser, C., Tomas, R., & Sun, L. (2015, Mar). The role of ocean-atmosphere coupling  
844 in the zonal-mean atmospheric response to Arctic sea ice loss. *Journal of Cli-*  
845 *mate*, 28, 2168–2186.
- 846 DuVivier, A., Holland, M., Kay, J., Tilmes, S., Gettelman, A., & Bailey, D. (2019,  
847 submitted). Arctic and Antarctic sea ice state in the Community Earth System  
848 Model version 2. *Journal of Geophysical Research: Oceans*.
- 849 Eicken, H. (2003). Sea ice: an introduction to its physics, chemistry, biology and ge-  
850 ology. In (p. 22-81). Wiley Online Library.
- 851 Eicken, H., Fischer, H., & Lemke, P. (1995). Effects of the snow cover on Antarc-  
852 tic sea ice and potential modulation of its response to climate change. *Annals*  
853 *of Glaciology*, 21, 369–376.
- 854 England, M., Polvani, L., & Sun, L. (2018). Contrasting the Antarctic and Arctic  
855 atmospheric responses to projected sea ice loss in the late twenty-first century.  
856 *Journal of Climate*, 31(16), 6353–6370.
- 857 Feltham, D., Untersteiner, N., Wettlaufer, J., & Worster, M. (2006). Sea ice is a  
858 mushy layer. *Geophysical Research Letters*, 33(14).
- 859 Garrison, D., & Buck, K. (1989). The biota of Antarctic pack ice in the Weddell Sea  
860 and Antarctic Peninsula regions. *Polar Biology*, 10(3), 211–219.
- 861 Gettelman, A., & Morrison, H. (2015). Advanced two-moment bulk microphysics for  
862 global models. Part I: Off-line tests and comparison with other schemes. *Jour-*  
863 *nal of Climate*, 28(3), 1268–1287.
- 864 Gettelman, A., Morrison, H., Santos, S., Bogenschutz, P., & Caldwell, P. (2015).  
865 Advanced two-moment bulk microphysics for global models. Part II: Global  
866 model solutions and aerosol–cloud interactions. *Journal of Climate*, 28(3),  
867 1288–1307.

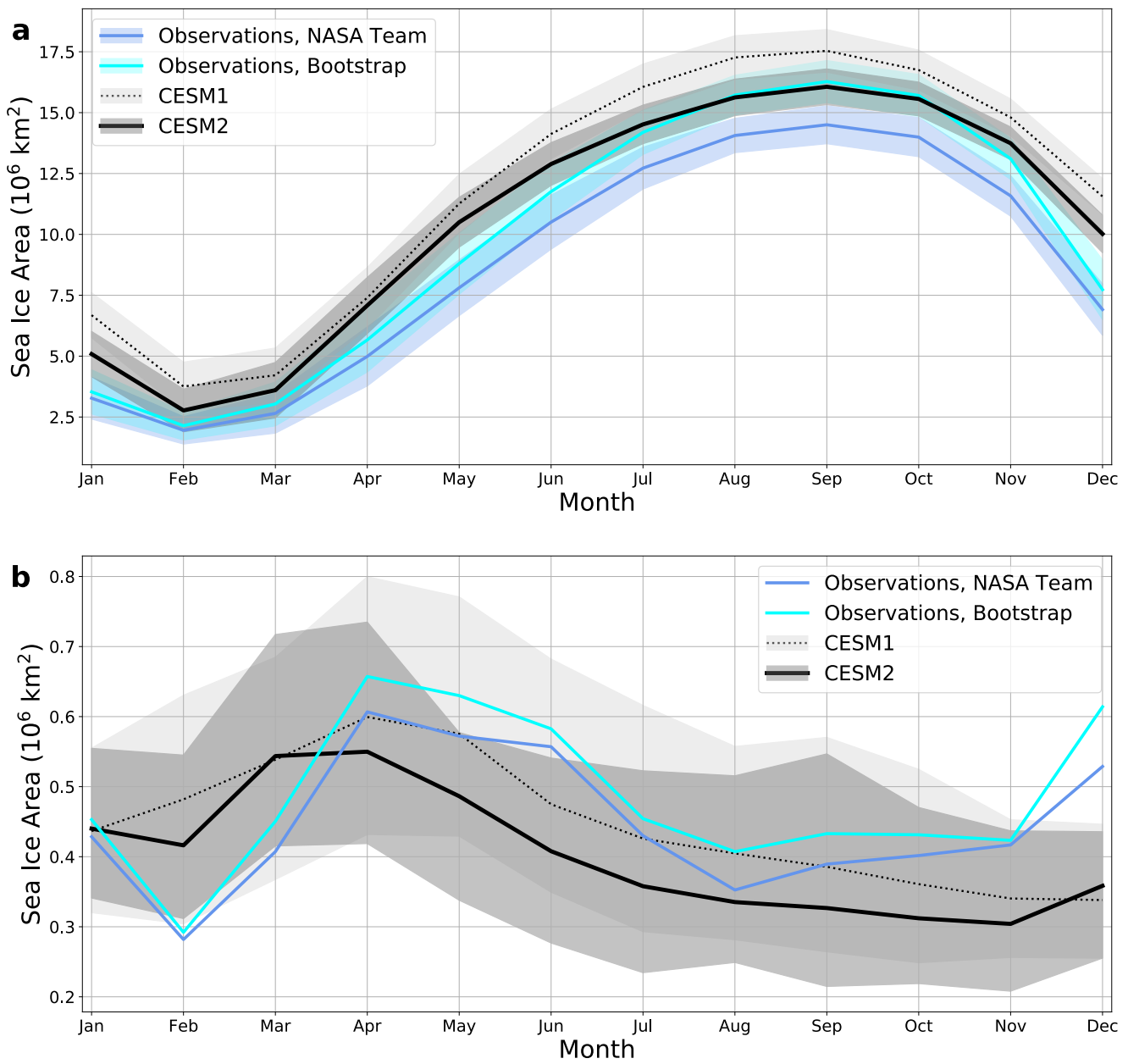
- 868 Goosse, H., Campin, J.-M., Fichefet, T., & Deleersnijder, E. (1997). Impact of sea-  
869 ice formation on the properties of Antarctic Bottom Water. *Annals of Glaciology*,  
870 *25*, 276–281.
- 871 Gordon, A. (1981). Seasonality of Southern Ocean sea ice. *Journal of Geophysical*  
872 *Research: Oceans*, *86*(C5), 4193–4197.
- 873 Guo, H., Golaz, J.-C., Donner, L., Wyman, B., Zhao, M., & Ginoux, P. (2015).  
874 CLUBB as a unified cloud parameterization: Opportunities and challenges.  
875 *Geophysical Research Letters*, *42*(11), 4540–4547.
- 876 Holland, M., & Bitz, C. (2003). Polar amplification of climate change in coupled  
877 models. *Climate Dynamics*, *21*, 221–232.
- 878 Holland, M., Landrum, L., Kostov, Y., & Marshall, J. (2017). Sensitivity of Antarc-  
879 tic sea ice to the Southern Annular Mode in coupled climate models. *Climate*  
880 *Dynamics*, *49*, 1813–1831.
- 881 Holland, M., Landrum, L., Raphael, M., & Kwok, R. (2018). The regional, seasonal,  
882 and lagged influence of the Amundsen Sea Low on Antarctic sea ice. *Geophysi-*  
883 *cal Research Letters*, *45*(20), 11–227.
- 884 Hoose, C., Kristjánsson, J., Chen, J.-P., & Hazra, A. (2010). A classical-theory-  
885 based parameterization of heterogeneous ice nucleation by mineral dust, soot,  
886 and biological particles in a global climate model. *Journal of the Atmospheric*  
887 *Sciences*, *67*(8), 2483–2503.
- 888 Hunke, E., & Lipscomb, W. (2008). *CICE: the Los Alamos sea ice model, documen-*  
889 *tation and software, version 4.0* (Tech. Rep. No. LA-CC-06-012). Los Alamos  
890 National Laboratory.
- 891 Hunke, E., Lipscomb, W., Turner, A., Jeffery, N., & Elliott, S. (2015). *CICE: the*  
892 *Los Alamos sea ice model, documentation and software, version 5.1* (Tech.  
893 Rep. No. LA-CC-06-012). T-E Fluid Dynamics Group, Los Alamos National  
894 Laboratory.
- 895 Jeffries, M., Kruse, H., Hurst-Cushing, B., & Maksym, T. (2001). Snow-ice ac-  
896 cretion and snow-cover depletion on Antarctic first-year sea-ice floes. *Annals of*  
897 *Glaciology*, *33*, 51–60.
- 898 Kay, J., Deser, C., Phillips, A., Mai, A., Hannay, C., Strand, G., ... Vertenstein,  
899 M. (2015). The Community Earth System Model (CESM) Large Ensemble  
900 project: A community resource for studying climate change in the presence of

- internal climate variability. *Bulletin of the American Meteorological Society*, *96*, 1333–1349.
- Kwok, R., & Comiso, J. (2002). Southern Ocean climate and sea ice anomalies associated with the Southern Oscillation. *Journal of Climate*, *15*(5), 487–501.
- Larson, V. (2017). CLUBB-SILHS: A parameterization of subgrid variability in the atmosphere. *arXiv preprint arXiv:1711.03675*.
- Leppäranta, M. (1993). A review of analytical models of sea-ice growth. *Atmosphere-Ocean*, *31*(1), 123–138.
- Maksym, T., & Markus, T. (2008). Antarctic sea ice thickness and snow-to-ice conversion from atmospheric reanalysis and passive microwave snow depth. *Journal of Geophysical Research: Oceans*, *113*(C2).
- Maqueda, M. M., Willmott, A., & Biggs, N. (2004). Polynya dynamics: A review of observations and modeling. *Reviews of Geophysics*, *42*(1).
- Massom, R., Eicken, H., Hass, C., Jeffries, M., Drinkwater, M., Sturm, M., ... others (2001). Snow on Antarctic sea ice. *Reviews of Geophysics*, *39*(3), 413–445.
- Massom, R., Scambos, T., Bennetts, L., Reid, P., Squire, V., & Stammerjohn, S. (2018). Antarctic ice shelf disintegration triggered by sea ice loss and ocean swell. *Nature*, *558*(7710), 383–389.
- Maykut, G., & Untersteiner, N. (1971). Some results from a time-dependent thermodynamic model of sea ice. *Journal of Geophysical Research*, *76*(6), 1550–1575.
- McGraw, M., & Barnes, E. (2016). Seasonal sensitivity of the eddy-driven jet to tropospheric heating in an idealized AGCM. *Journal of Climate*, *29*, 5223–5240.
- Meehl, G., Arblaster, J., Bitz, C., Chung, C., & Teng, H. (2016). Antarctic sea-ice expansion between 2000 and 2014 driven by tropical Pacific decadal climate variability. *Nature Geoscience*, *9*(8), 590–595.
- Morrison, A., Kay, J., Chepfer, H., Guzman, R., & Yettella, V. (2018). Isolating the liquid cloud response to recent arctic sea ice variability using spaceborne lidar observations. *Journal of Geophysical Research: Atmospheres*, *123*(1), 473–490.
- Ohshima, K., Fukamachi, Y., Williams, G., Nihashi, S., Roquet, F., Kitade, Y., ... others (2013). Antarctic Bottom Water production by intense sea-ice formation in the Cape Darnley polynya. *Nature Geoscience*, *6*(3), 235–240.
- Parkinson, C., & Cavalieri, D. (2012). Antarctic sea ice variability and trends, 1979–2010. *The Cryosphere*, *6*, 871–880.

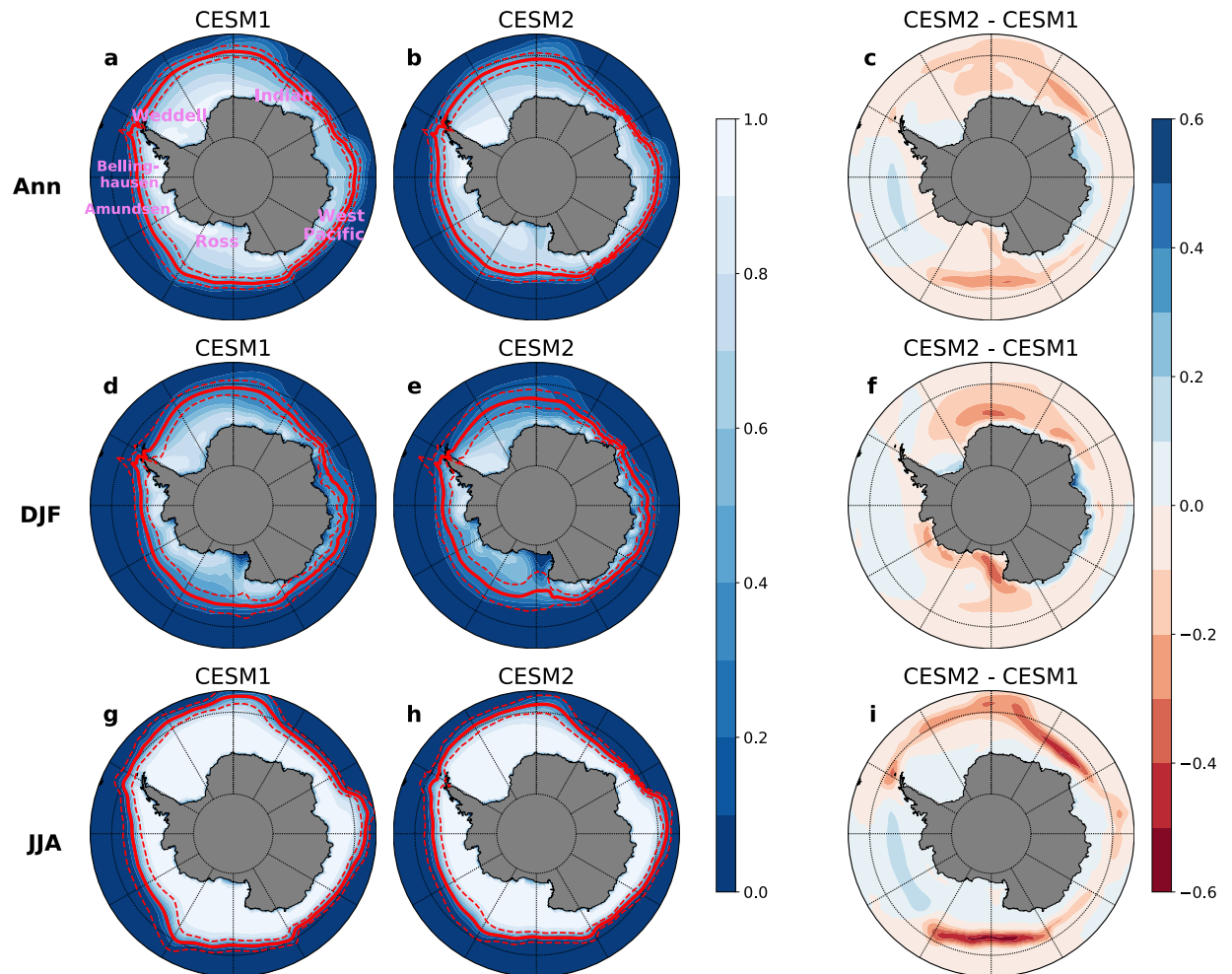
- 934 Pauling, A., Bitz, C., Smith, I., & Langhorne, P. (2016). The response of the South-  
935 ern Ocean and Antarctic sea ice to freshwater from ice shelves in an Earth  
936 System Model. *Journal of Climate*, 29, 1655–1672.
- 937 Pellichero, V., Sallée, J.-B., Schmidtko, S., Roquet, F., & Charrassin, J.-B. (2017).  
938 The ocean mixed layer under Southern Ocean sea-ice: Seasonal cycle and  
939 forcing. *Journal of Geophysical Research: Oceans*, 122(2), 1608–1633.
- 940 Perovich, D., Richter-Menge, J., Polashenski, C., Elder, B., Arbesser, T., & Bren-  
941 nick, O. (2014). Sea ice mass balance observations from the North Pole  
942 Environmental Observatory. *Geophysical Research Letters*, 41(6), 2019–2025.
- 943 Powell, D., Markus, T., & Stössel, A. (2005). Effects of snow depth forcing on  
944 Southern Ocean sea ice simulations. *Journal of Geophysical Research: Oceans*,  
945 110(C6).
- 946 Raphael, M. (2004). A zonal wave 3 index for the Southern Hemisphere. *Geophysical  
947 Research Letters*, 31(23).
- 948 Raphael, M. (2007). The influence of atmospheric zonal wave three on Antarctic sea  
949 ice variability. *Journal of Geophysical Research: Atmospheres*, 112(D12).
- 950 Raphael, M., & Hobbs, W. (2014). The influence of the large-scale atmospheric cir-  
951 culation on Antarctic sea ice during ice advance and retreat seasons. *Geophysi-  
952 cal Research Letters*, 41(14), 5037–5045.
- 953 Roach, L. A., Dörr, J., Holmes, C. R., Massonnet, F., Blockley, E. W., Notz, D., ...  
954 others (2020). Antarctic sea ice area in CMIP6. *Geophysical Research Letters*,  
955 47(9), e2019GL086729.
- 956 Rothrock, D., Yu, Y., & Maykut, G. (1999). Thinning of the Arctic sea-ice cover.  
957 *Geophysical Research Letters*, 26(23), 3469–3472.
- 958 Scinocca, J., & McFarlane, N. (2000). The parametrization of drag induced by strat-  
959 ified flow over anisotropic orography. *Quarterly Journal of the Royal Meteorolo-  
960 gical Society*, 126(568), 2353–2393.
- 961 Shi, X., Liu, X., & Zhang, K. (2015). Effects of pre-existing ice crystals on cir-  
962 rus clouds and comparison between different ice nucleation parameterizations  
963 with the community atmosphere model (CAM5). *Atmospheric Chemistry and  
964 Physics (Online)*, 15(PNNL-SA-103838).
- 965 Sigmond, M., & Fyfe, J. (2010). Has the ozone hole contributed to increased Antarc-  
966 tic sea ice extent? *Geophysical Research Letters*, 37(L18502).

- 967 Simpkins, G., Ciasto, L., Thompson, D., & England, M. (2012). Seasonal relationships between large-scale climate variability and Antarctic sea ice concentration. *Journal of Climate*, 25(16), 5451–5469.
- 970 Singh, H., Garuba, O., & Rasch, P. (2018). How asymmetries between Arctic and  
971 Antarctic climate sensitivity are modified by the ocean. *Geophysical Research  
972 Letters*, 45(23), 13-31.
- 973 Singh, H., Polvani, L., & Rasch, P. (2019). Antarctic sea ice expansion, driven by  
974 internal variability, in the presence of increasing atmospheric CO<sub>2</sub>. *Geophysical  
975 Research Letters*(doi: 10.1029/2019GL083758).
- 976 Smith, D., Dunstone, N., Scaife, A., Fiedler, E., Copsey, D., & Hardiman, S. (2017).  
977 Atmospheric response to Arctic and Antarctic sea ice: The importance of  
978 ocean–atmosphere coupling and the background state. *Journal of Climate*,  
979 30(12), 4547–4565.
- 980 Swart, N., & Fyfe, J. (2013). The influence of recent Antarctic ice sheet retreat on  
981 simulated sea ice area trends. *Geophysical Research Letters*, 40, 4328-4332.
- 982 Swart, N., Fyfe, J., Hawkins, E., Kay, J., & Jahn, A. (2015). Influence of internal  
983 variability on Arctic sea-ice trends. *Nature Climate Change*, 5(2), 86.
- 984 Tamura, T., Ohshima, K., & Nihashi, S. (2008). Mapping of sea ice production for  
985 Antarctic coastal polynyas. *Geophysical Research Letters*, 35(7).
- 986 Tamura, T., Ohshima, K. I., Fraser, A. D., & Williams, G. D. (2016). Sea  
987 ice production variability in Antarctic coastal polynyas. *Journal of Geo-  
988 physical Research: Oceans*, 121(5), 2967-2979. Retrieved from <https://agupubs.onlinelibrary.wiley.com/doi/abs/10.1002/2015JC011537> doi:  
989 10.1002/2015JC011537
- 990 Thorndike, A. (1992). A toy model linking atmospheric thermal radiation and sea  
991 ice growth. *Journal of Geophysical Research*, 97(C6), 9401-9410.
- 992 Turner, A., & Hunke, E. (2015). Impacts of a mushy-layer thermodynamic ap-  
993 proach in global sea-ice simulations using the CICE sea-ice model. *Journal of  
994 Geophysical Research: Oceans*, 120(2), 1253–1275.
- 995 Turner, A., Hunke, E., & Bitz, C. (2013). Two modes of sea-ice gravity drainage:  
996 A parameterization for large-scale modeling. *Journal of Geophysical Research:  
997 Oceans*, 118(5), 2279–2294.
- 998 Turner, J., Comiso, J., Marshall, G., Lachlan-Cope, T., Bracegirdle, T., Maksym, T.,

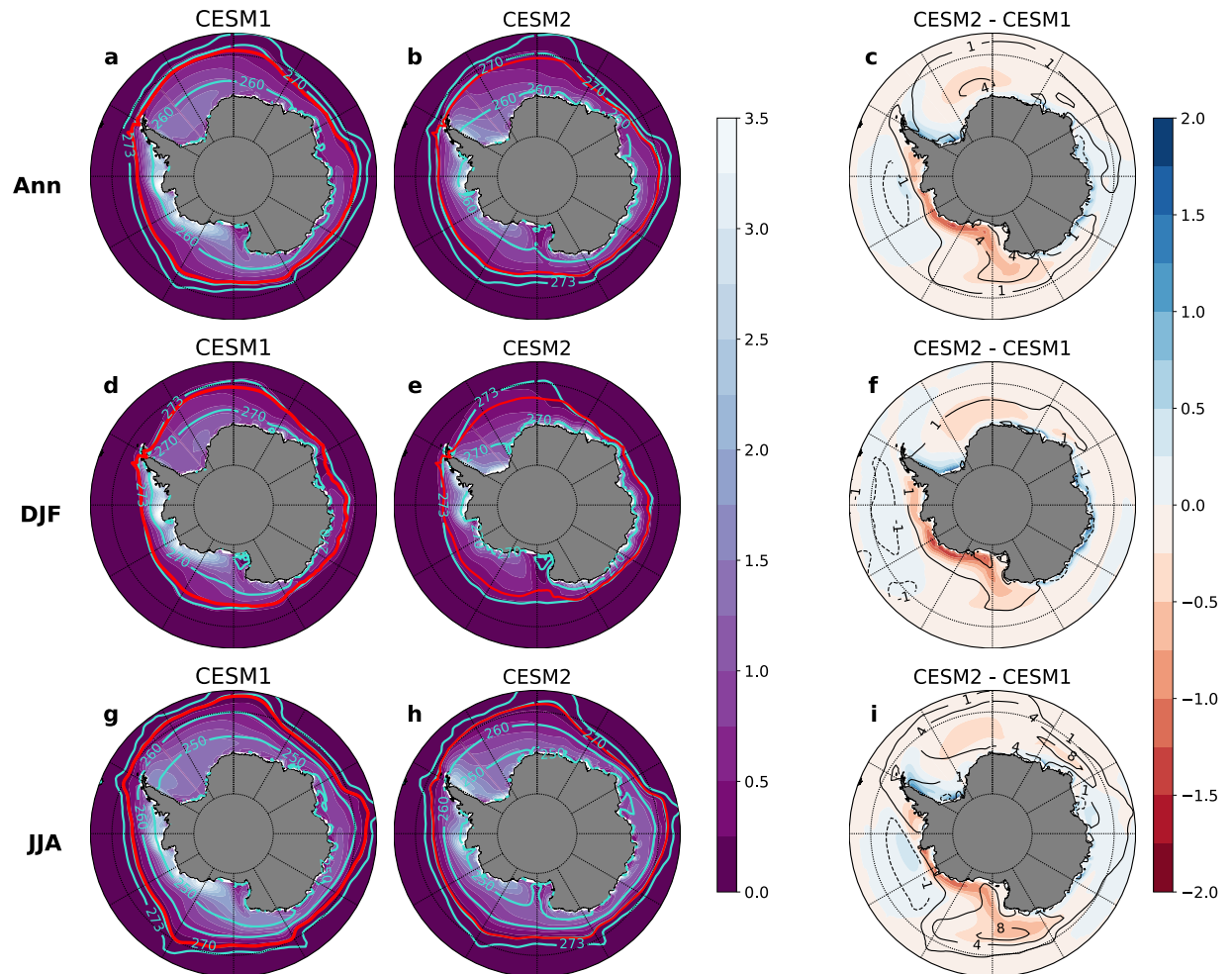
- 1000        ... Orr, A. (2009). Non-annular atmospheric circulation change induced by  
1001        stratospheric ozone depletion and its role in the recent increase in Antarctic  
1002        sea ice extent. *Geophysical Research Letters*, 36(L08502).
- 1003        Vancoppenolle, M., Fichefet, T., & Goosse, H. (2009). Simulating the mass balance  
1004        and salinity of Arctic and Antarctic sea ice. 2. importance of sea ice salinity  
1005        variations. *Ocean Modelling*, 27(1-2), 54–69.
- 1006        Wall, C., Kohyama, T., & Hartmann, D. (2017). Low-cloud, boundary layer, and sea  
1007        ice interactions over the Southern Ocean during winter. *Journal of Climate*,  
1008        30, 4857-4871.
- 1009        Wang, Y., Liu, X., Hoose, C., & Wang, B. (2014). Different contact angle distribu-  
1010        tions for heterogeneous ice nucleation in the Community Atmospheric Model  
1011        version 5. *Atmospheric Chemistry and Physics*, 14(19), 10411–10411.
- 1012        Worby, A. P., Geiger, C. A., Paget, M. J., Van Woert, M. L., Ackley, S. F., & De-  
1013        Liberty, T. L. (2008). Thickness distribution of Antarctic sea ice. *Jour-*  
1014        *nal of Geophysical Research: Oceans*, 113(C5). Retrieved from <https://agupubs.onlinelibrary.wiley.com/doi/abs/10.1029/2007JC004254> doi:  
1015        10.1029/2007JC004254
- 1016        Zhang, L., Delworth, T., Cooke, W., & Yang, X. (2019). Natural variability of  
1017        Southern Ocean convection as a driver of observed climate trends. *Nature*  
1018        *Climate Change*, 9(1), 59.



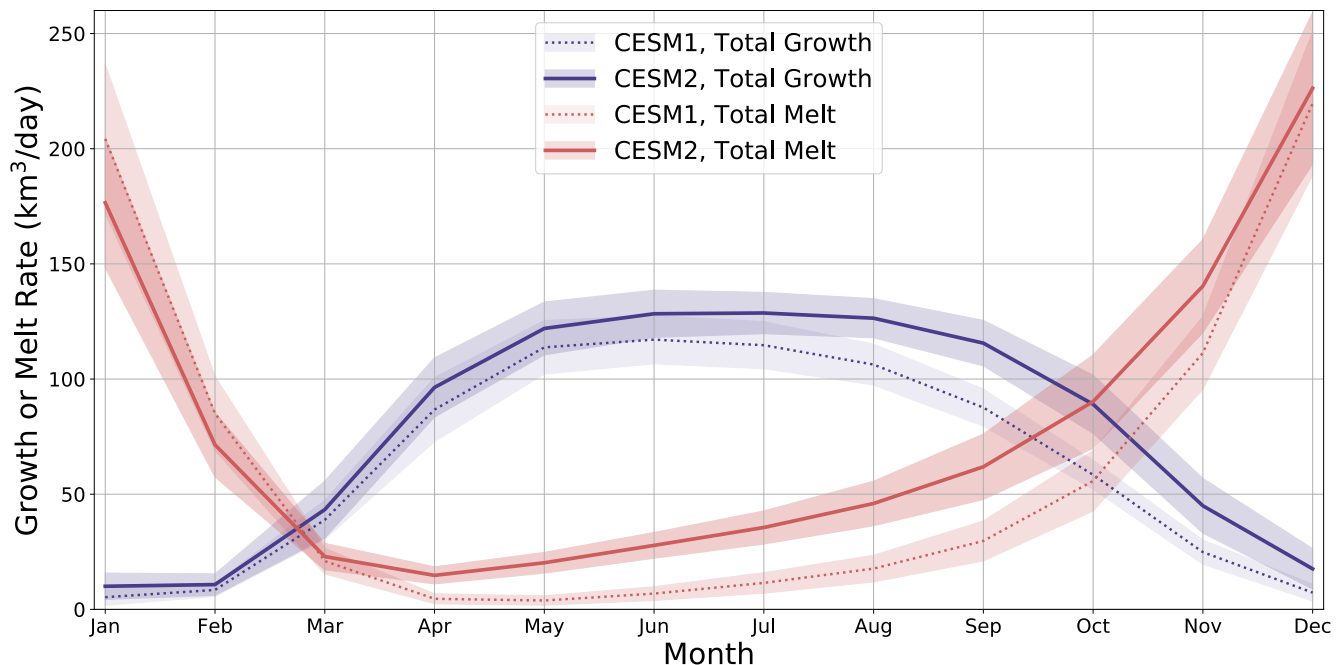
**Figure 1. Seasonal Cycle of Sea Ice Area:** (a) Monthly mean sea ice area, and (b) one standard deviation of the monthly sea ice area, both in  $10^6 \text{ km}^2$ . Shown for CESM2 (black, solid), CESM1 (black, dotted), and the satellite observations from 1979 to 2018 (blue and cyan). Shading in (a) provides the two standard deviation envelope for the variability in monthly ice area, while shading in (b) gives the range of the monthly standard deviation in each model, calculated for all contiguous 40-yr time periods in each 600-year pre-industrial run.



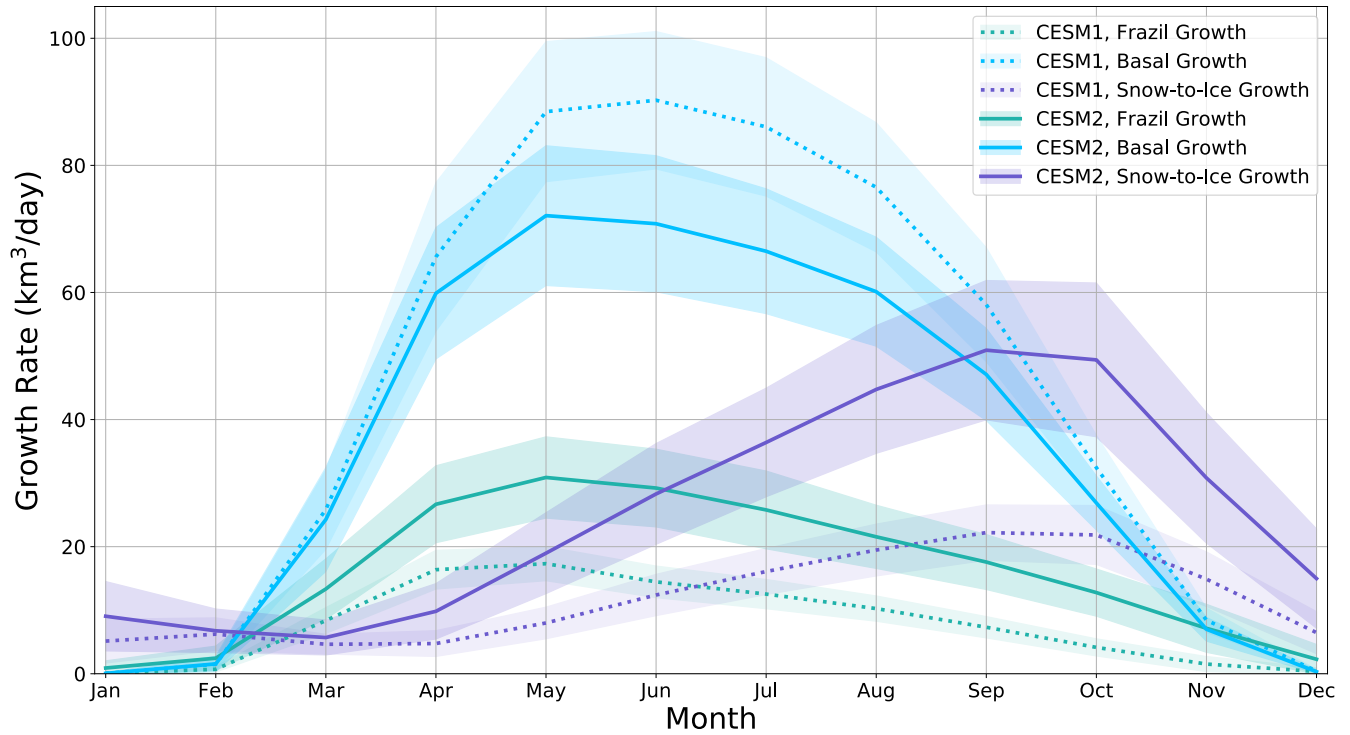
**Figure 2. Ice Fraction and Extent:** Sea ice fraction (colors) and sea ice extent (the 0.15 ice fraction isoline; thick red contour) in (a, d, g) CESM1 and (b, e, h) CESM2; panels (c, f, i) show the difference in sea ice fraction between CESM2 and CESM1 (colors). Shown for (a, b, c) the annual mean, (c, d, e) the December-January-February (DJF) mean, and (g, h, i) the June-July-August (JJA) mean. In the left and center columns, the dashed red contours show the one-standard-deviation envelope of the ice extent. Panel (a) indicates the sectors of the Antarctic referred to in the main text.



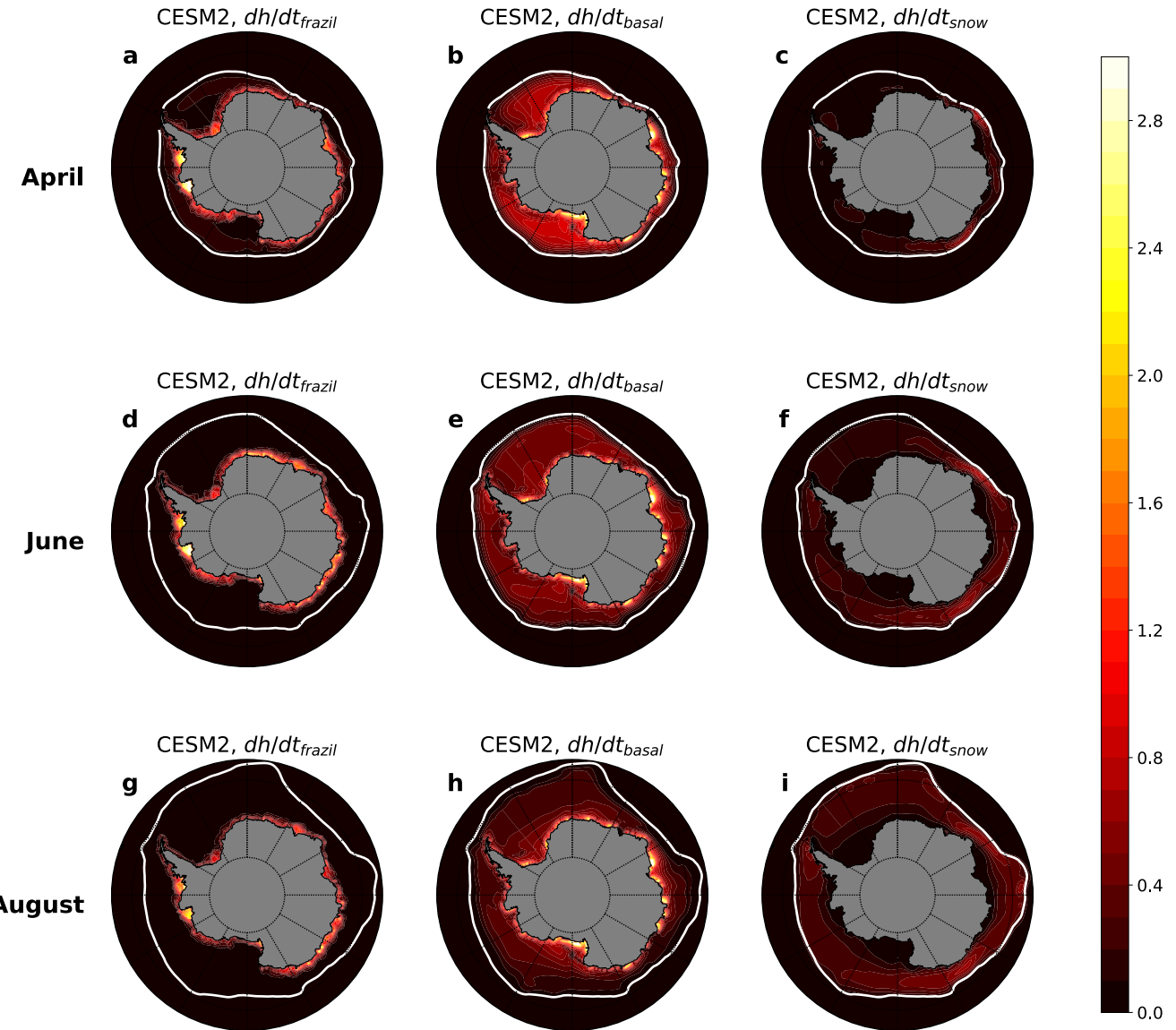
**Figure 3. Ice Thickness and Surface Temperature:** Sea ice thickness (in m; colors) and surface skin temperature (turquoise contours at [250, 260, 270, 273] K) in (a, e, h) CESM1 and (b, f, i) CESM2; panels (c, g, j) show differences between the CESM2 and CESM1 (temperature differences shown as black contours at [-1, 1, 4, 8] K; colors indicate ice thickness differences in m). Shown for (a, b, c) the annual mean, (d, e, f) the December-January-February (DJF) mean, and (g, h, i) the June-July-August (JJA) mean. In the left and center columns, the red contour shows the 0.15 ice fraction isoline.



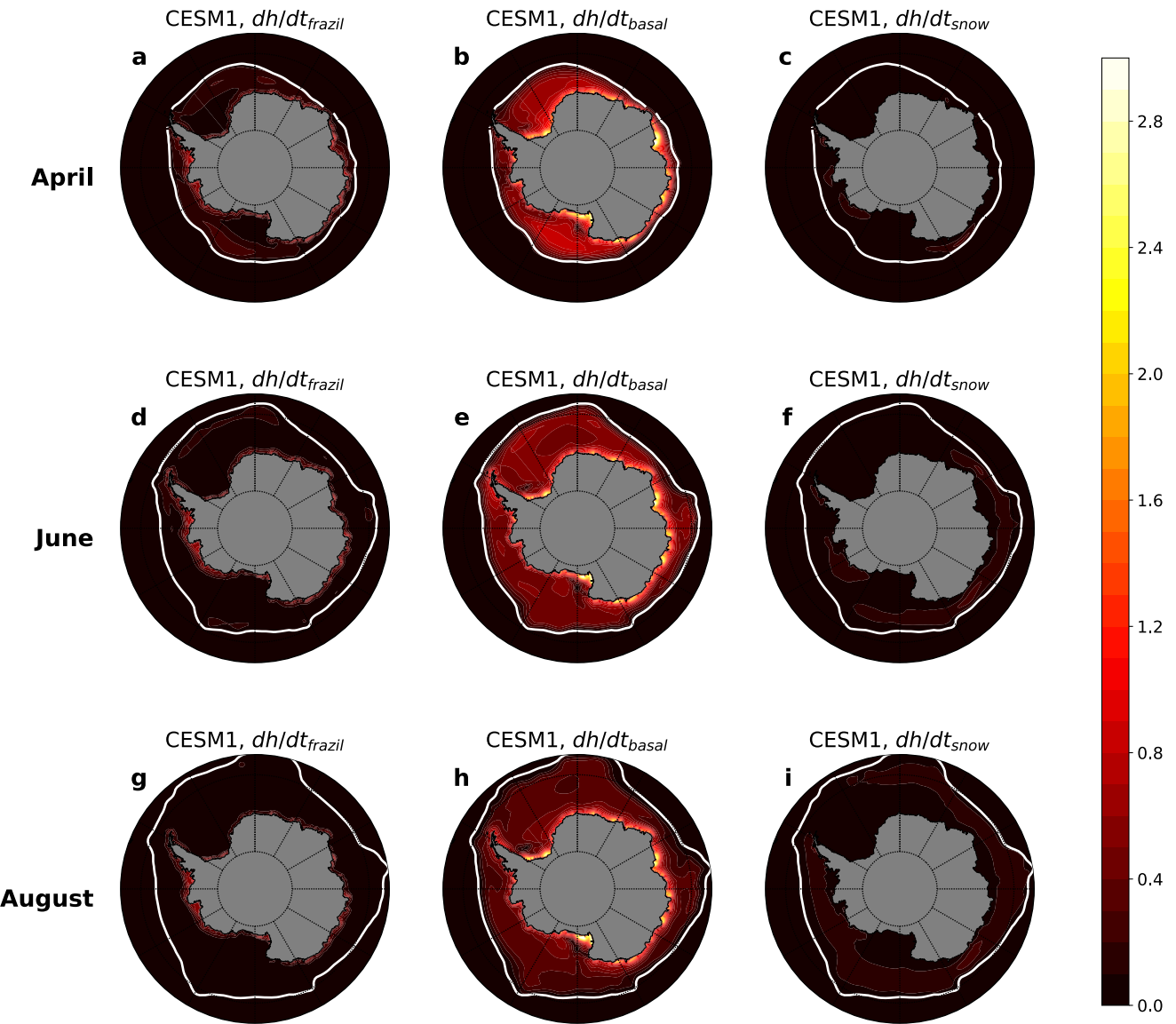
**Figure 4. Antarctic Sea Ice Growth and Melt Rates:** Monthly mean total sea ice growth rate (indigo lines) and melt rate (red lines) over the Antarctic in CESM2 (solid lines) and CESM1 (dotted lines), in  $\text{km}^3/\text{day}$ . Shaded envelopes show the one-standard-deviation range over each month in each model.



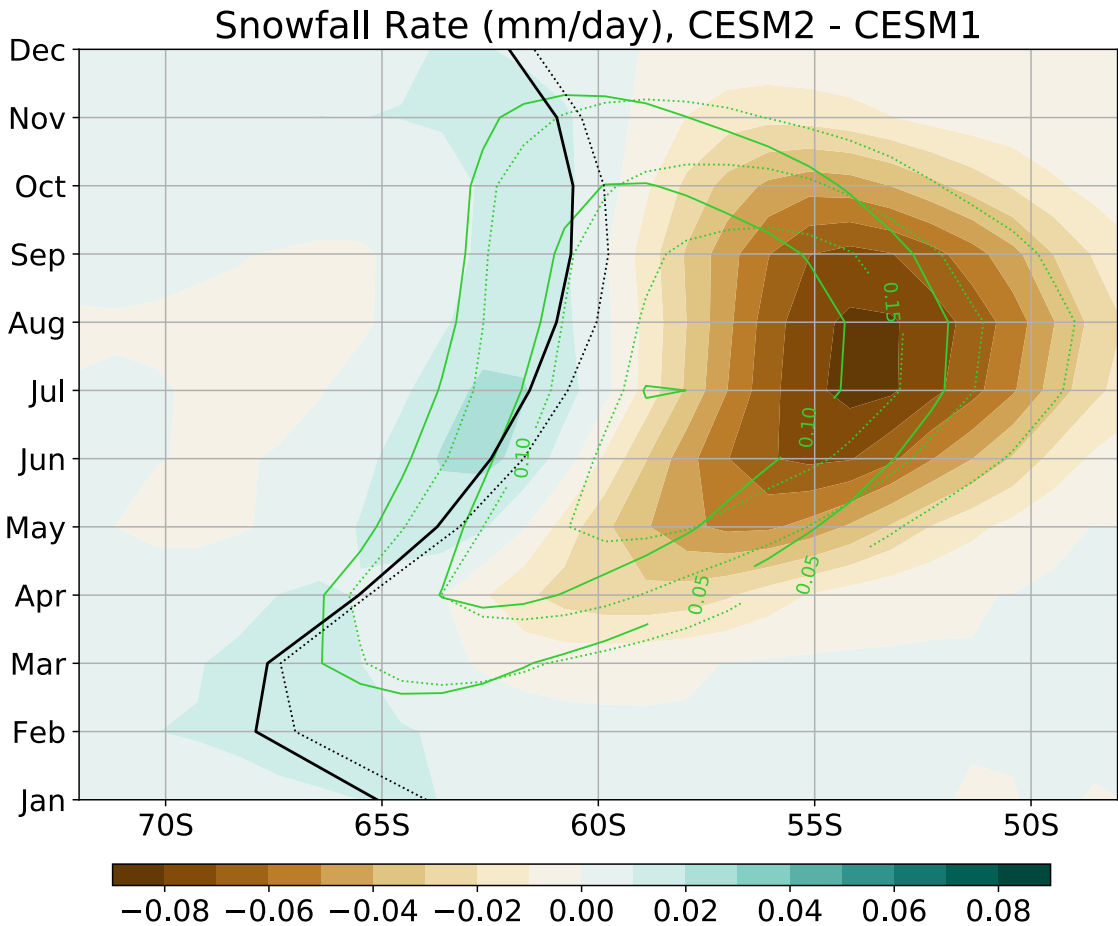
**Figure 5. Components of Antarctic Sea Ice Growth:** Monthly mean frazil growth (teal lines), basal growth (turquoise lines), and snow-to-ice growth (purple lines) in CESM2 (solid lines) and CESM1 (dotted lines), in  $\text{km}^3/\text{day}$ . Shaded envelopes show the one-standard-deviation range for each month and each model.



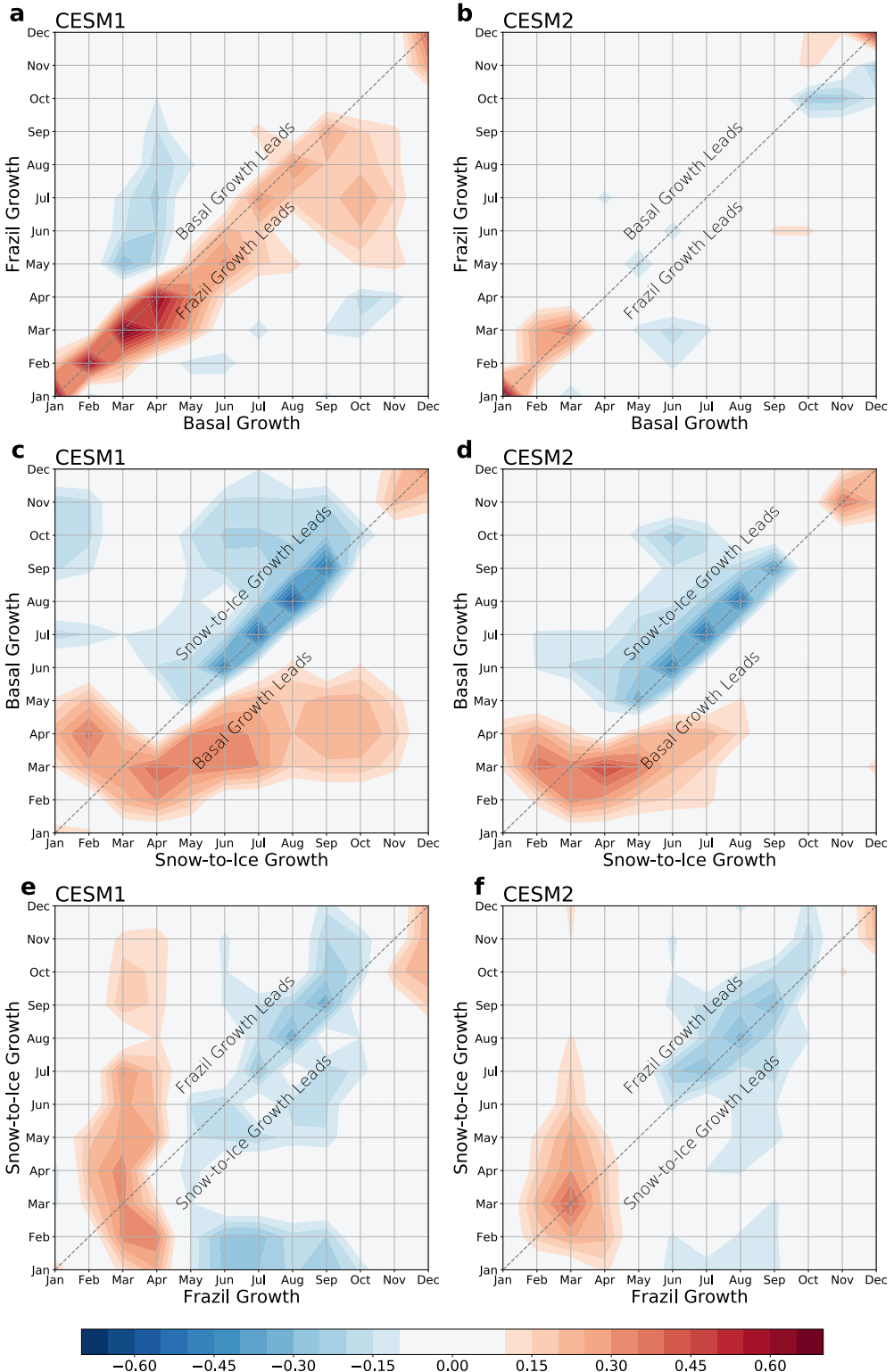
**Figure 6. Antarctic Sea Ice Growth in CESM2:** Monthly mean (a, d, g) frazil growth, (b, e, h) basal growth, and (c, f, i) snow-to-ice growth in (a, b, c) April, (d, e, f) June, and (g, h, i) August, in cm/day. In all panels, the white contour shows the 0.15 ice fraction isoline.



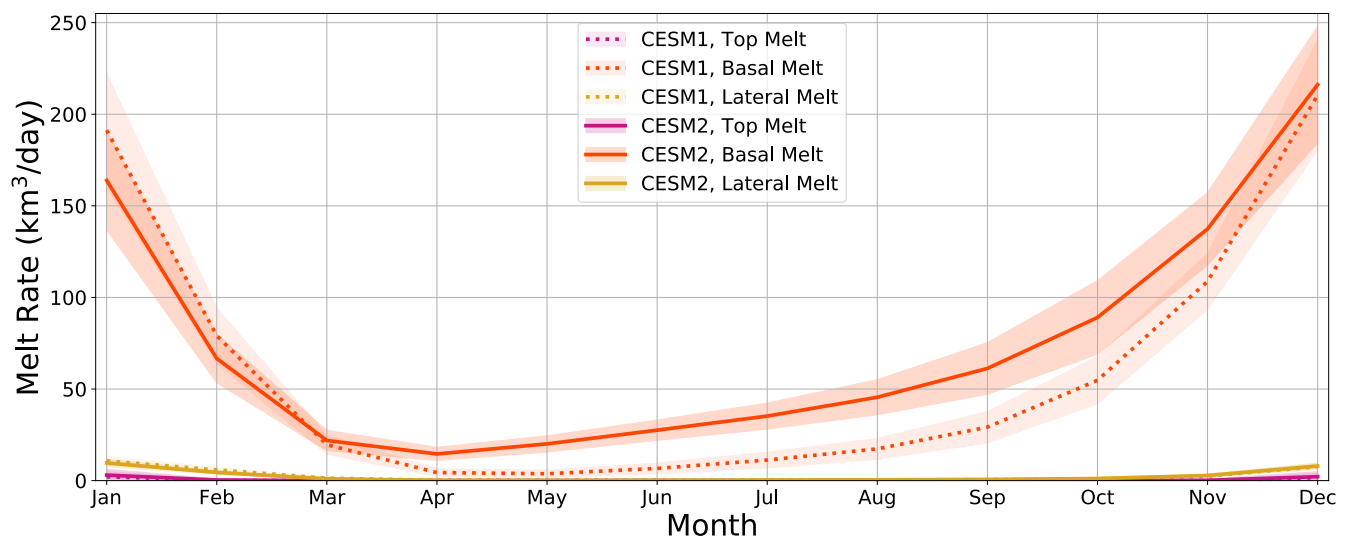
**Figure 7. Antarctic Sea Ice Growth in CESM1:** As in Fig 6, but for CESM1.



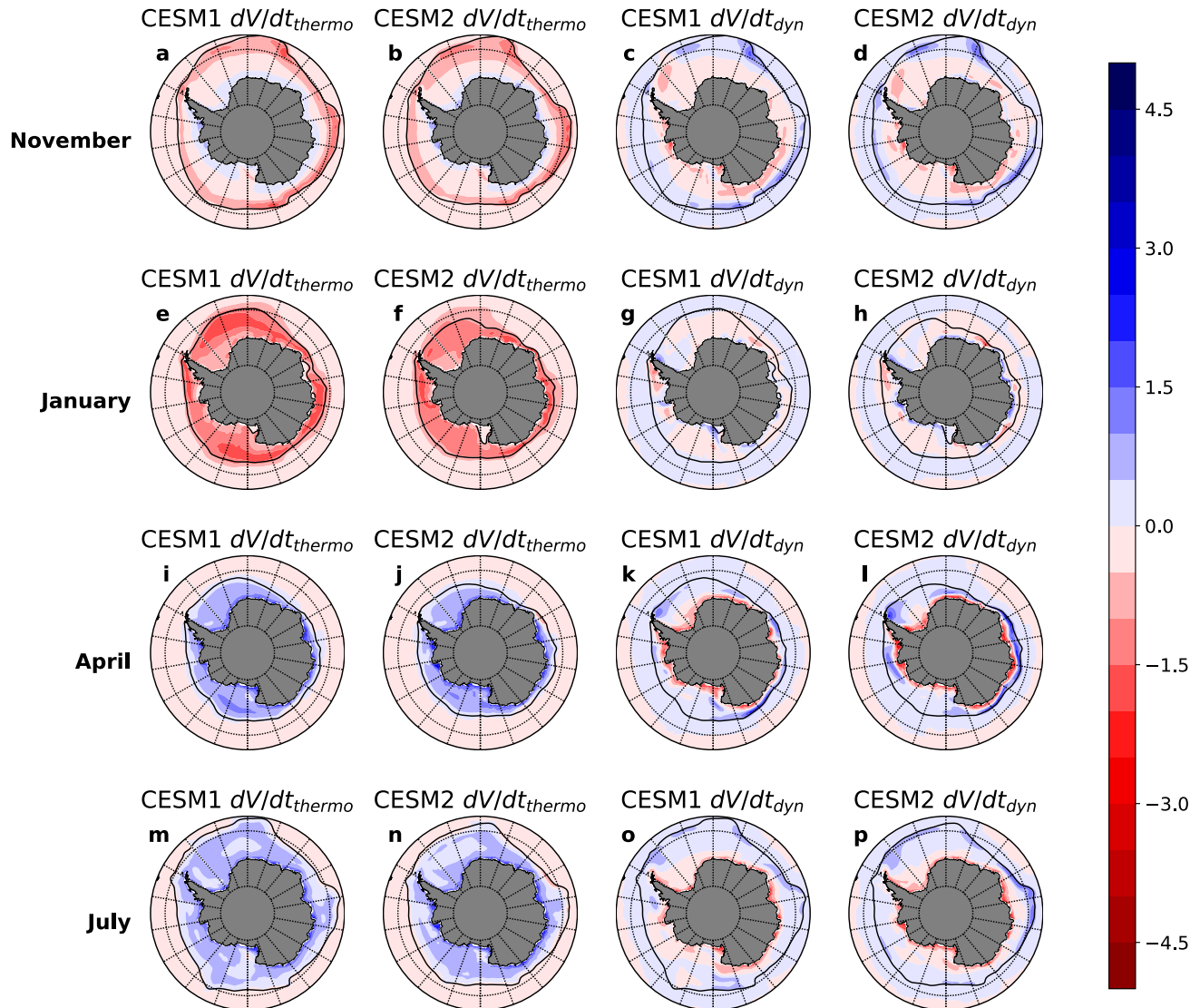
**Figure 8. Zonal Mean Monthly Snowfall Rate:** Difference between the monthly zonal mean snowfall rate in CESM2 and CESM1 (in mm/day; colors). Green solid and dotted contours (at 0.05, 0.1, and 0.15 mm/day) show the monthly zonal mean snowfall rates in CESM2 and CESM1, respectively. The monthly zonal mean ice extent (0.15 ice fraction isoline) for CESM2 (CESM1) is indicated by the solid (dotted) black contour.



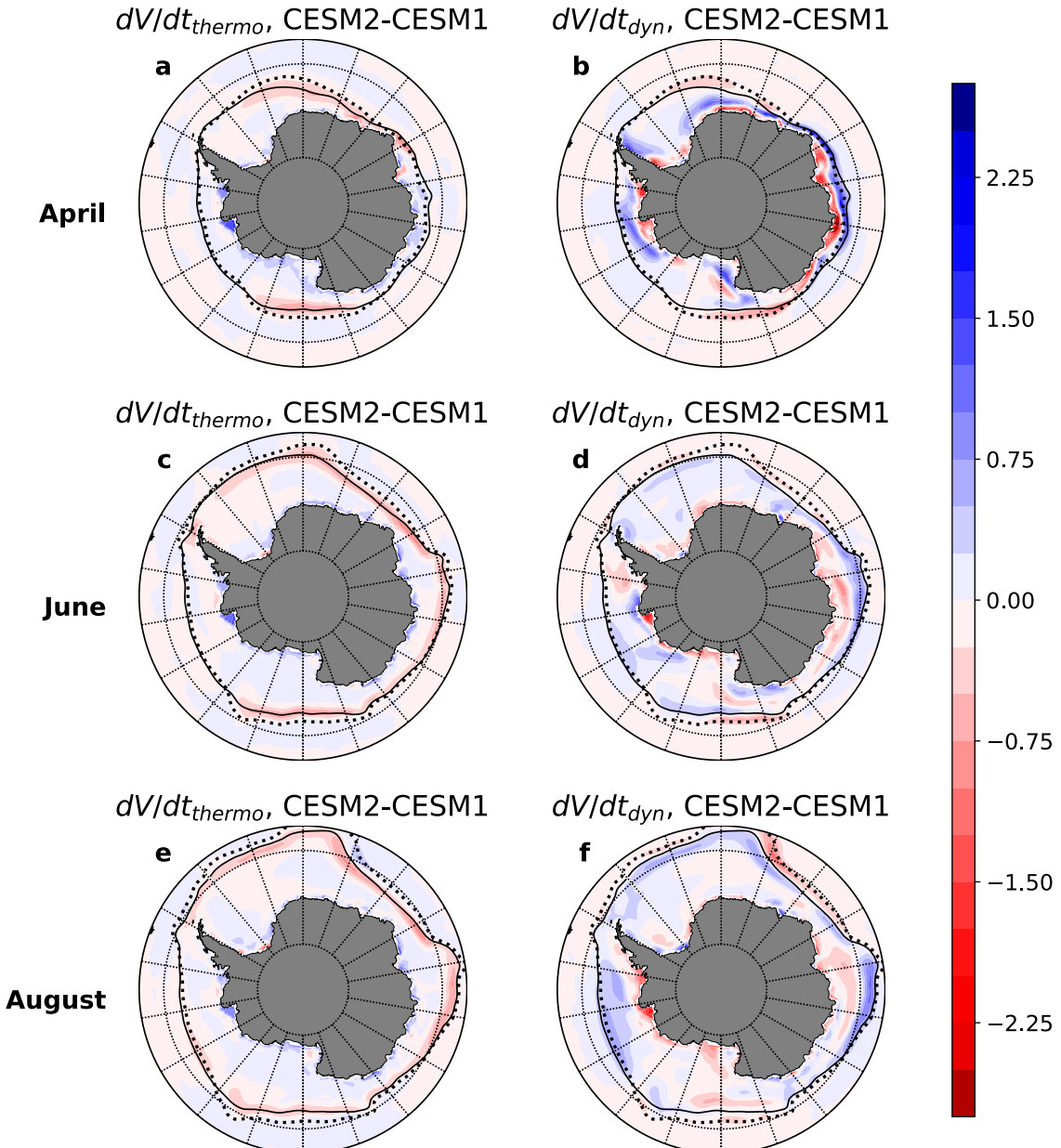
**Figure 9. Relationships Between Sea Ice Growth Terms:** Monthly lead-lag correlations between (a, b) frazil and basal growth, (c, d) basal and snow-to-ice growth, and (e, f) snow-to-ice and frazil growth in the (a, c, e) CESM1 and (b, d, f) CESM2. Only correlations that are statistically significant at  $p < 0.05$  are shown.



**Figure 10. Components of Antarctic Sea Ice Melt:** Monthly mean basal melt (red lines), lateral melt (gold lines), and top melt (purple lines) in CESM2 (solid lines) and CESM1 (dotted lines), in  $\text{km}^3/\text{day}$ . Shaded envelopes show the one-standard-deviation range in the melt term for each month and each model.

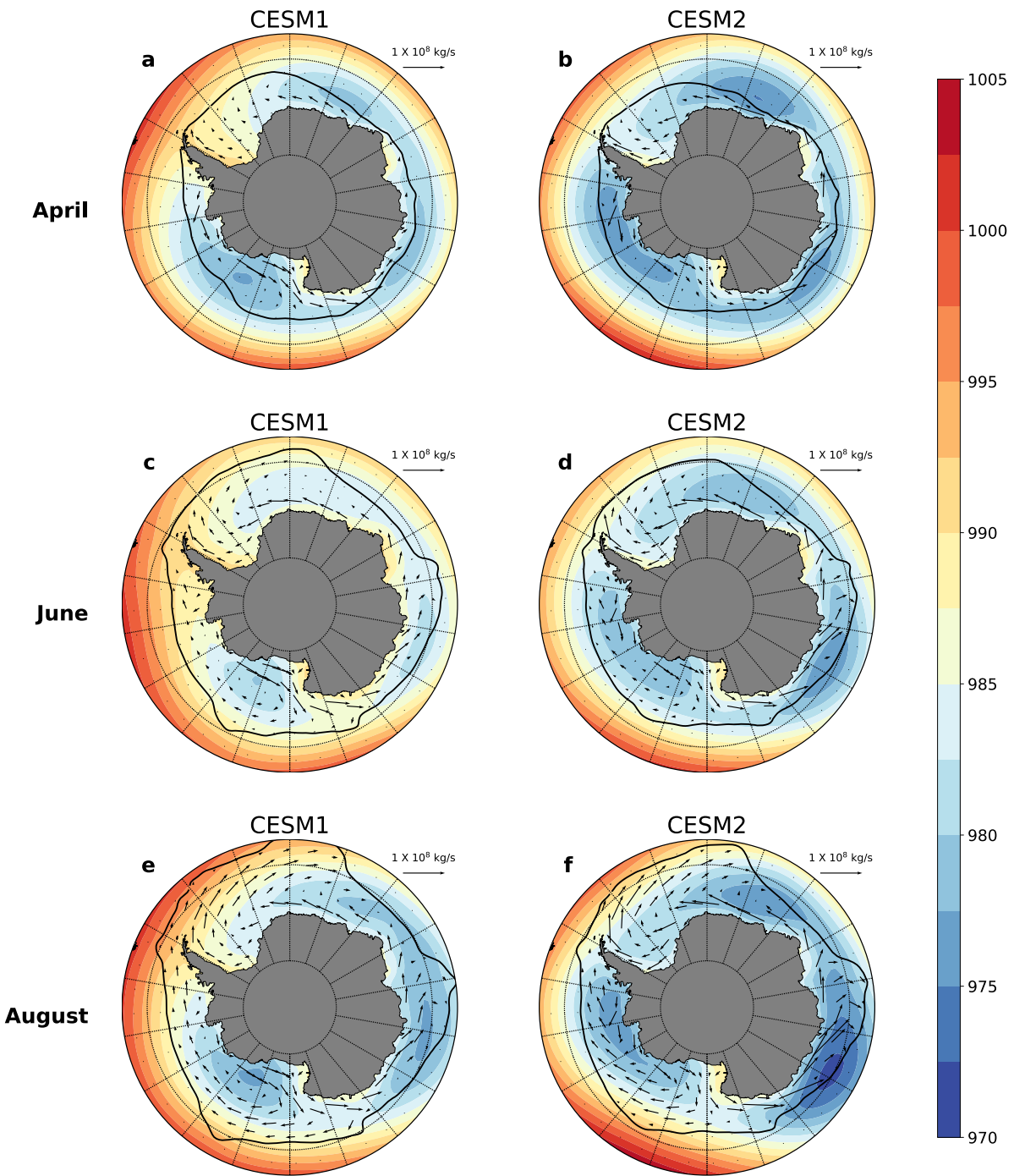


**Figure 11. Thermodynamic and Dynamic Contributions to Antarctic Sea Ice Volume Change:** Monthly mean (a, b, e, f, i, j, m, n) thermodynamic and (c, d, g, h, k, l, o, p) dynamic contributions to ice volume tendency  $dV/dt$ , in cm/day, in the (a, c, e, g, i, k, m, o) CESM1, and (b, d, f, h, j, l, n, p) CESM2. Shown for (a-d) November, (e-h) January, (i-l) April, and (m-p) July. In all panels, the black contour indicates sea ice extent (i.e. 0.15 ice fraction isoline).



**Figure 12. Differences in Thermodynamic and Dynamic Contributions to Antarctic Sea Ice Volume Change over the Growth Season in CESM2 versus CESM1:**

Monthly mean difference in the (a, c, e) thermodynamic and (b, d, f) dynamic contributions to ice volume tendency  $dV/dt$ , in cm/day, between CESM2 and CESM1 (i.e. CESM2 minus CESM1). Shown for (a, b) April, (c, d) June, and (e,f) August. In all panels, the solid black contour indicates sea ice extent in CESM2, and the dotted black contour indicates sea ice extent in CESM1.

**Figure 13.** Antarctic Sea Ice Transport and Sea Level Pressure during the Growth

**Season:** Monthly mean sea ice transport (vectors; scaled by  $10^8 \text{ kg/s}$ ) and sea level pressure (colors; in hPa) in the (a, c, e) CESM1 and (b, d, f) CESM2, in (a, b) April, (c, d) June, and (e, f) August.

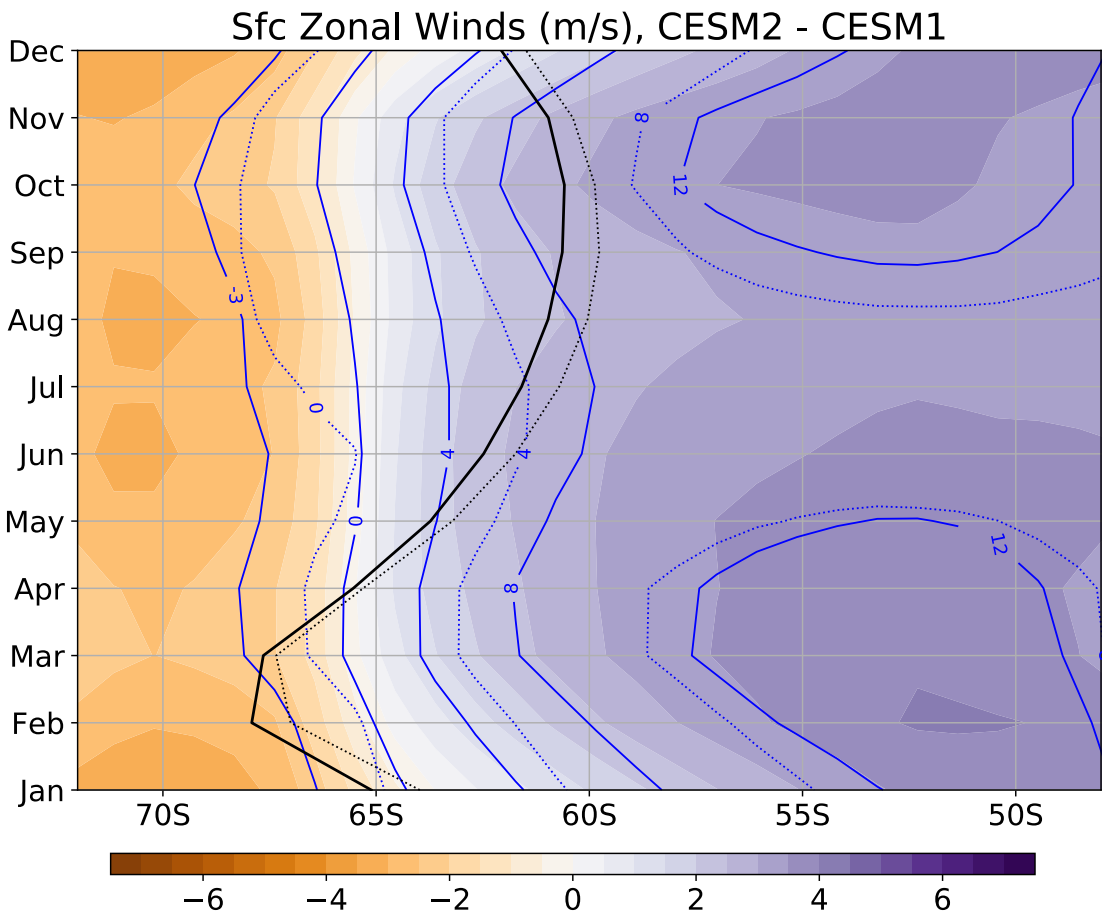


**Figure 14. Zonal Winds at the Surface:** Difference between the monthly zonal mean surface zonal winds in CESM2 and CESM1 (in m/sec; colors). Blue solid and dotted contours (at -3, 0, 4, 8, 12 m/s) show the monthly zonal mean surface zonal winds in CESM2 and CESM1, respectively. The monthly zonal mean ice extent (0.15 ice fraction isoline) for CESM2 (CESM1) is indicated by the solid (dotted) black contour.

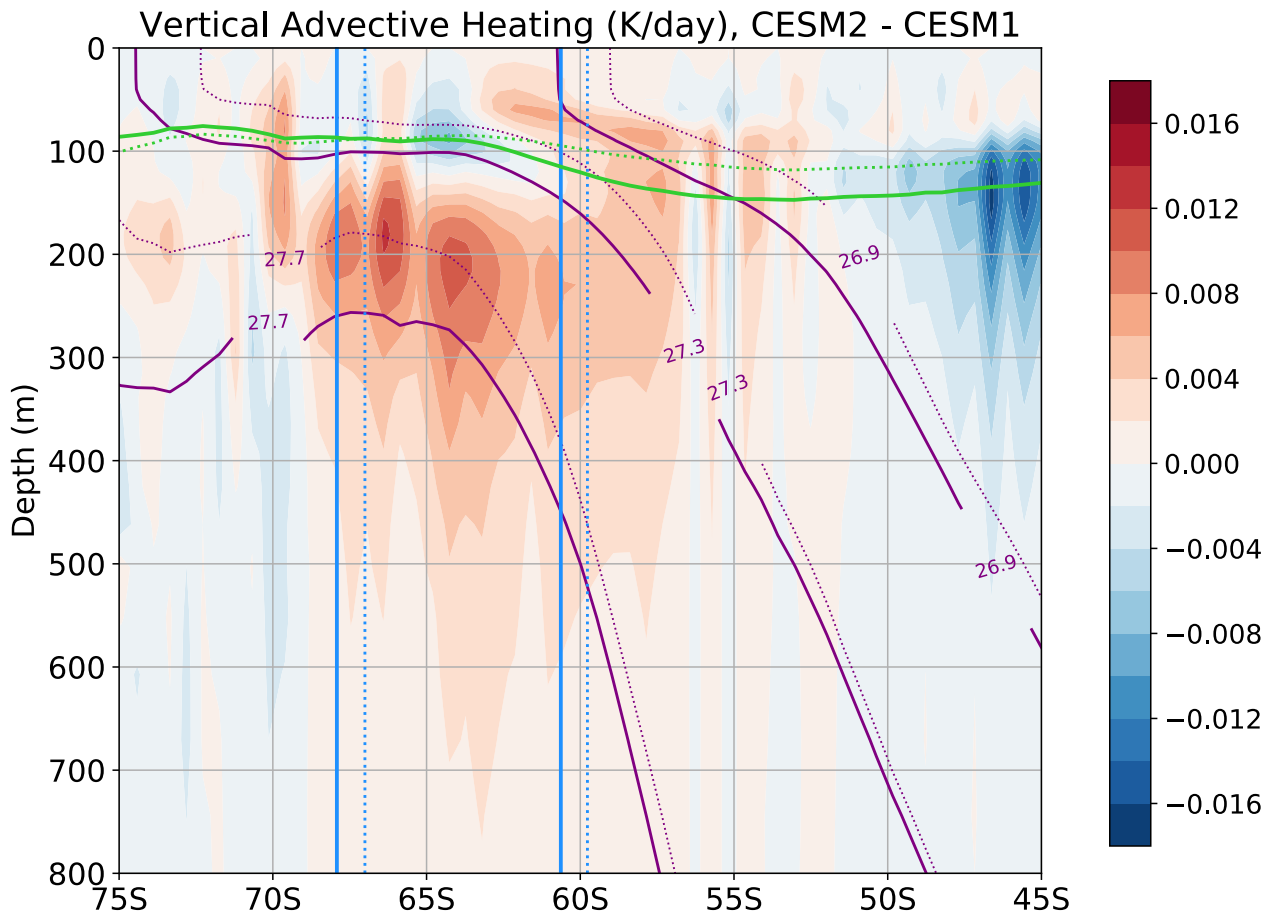


**Figure 15. Heating by Upwelling during the Sea Ice Growth Season:** Difference between ocean heating due to advection in CESM2 and CESM1 (in K/day; colors) over the growth season (March to August). Isopycnal surfaces (at  $\sigma = 27.7, 27.3, 26.9 \text{ kg/m}^3$ ) in CESM2 and CESM1 are shown by the purple solid and dotted contours, respectively. The blue solid (dotted) lines show the range of the ice extent in CESM2 (CESM1) from March to August, and the green solid (dotted) line indicates the zonal mean mixed layer depth in CESM2 (CESM1) over the growth season; the base of the mixed layer is reckoned as the depth where seawater density is  $0.125 \text{ kg/m}^3$  greater than that at the surface (see Danabasoglu et al., 2012).

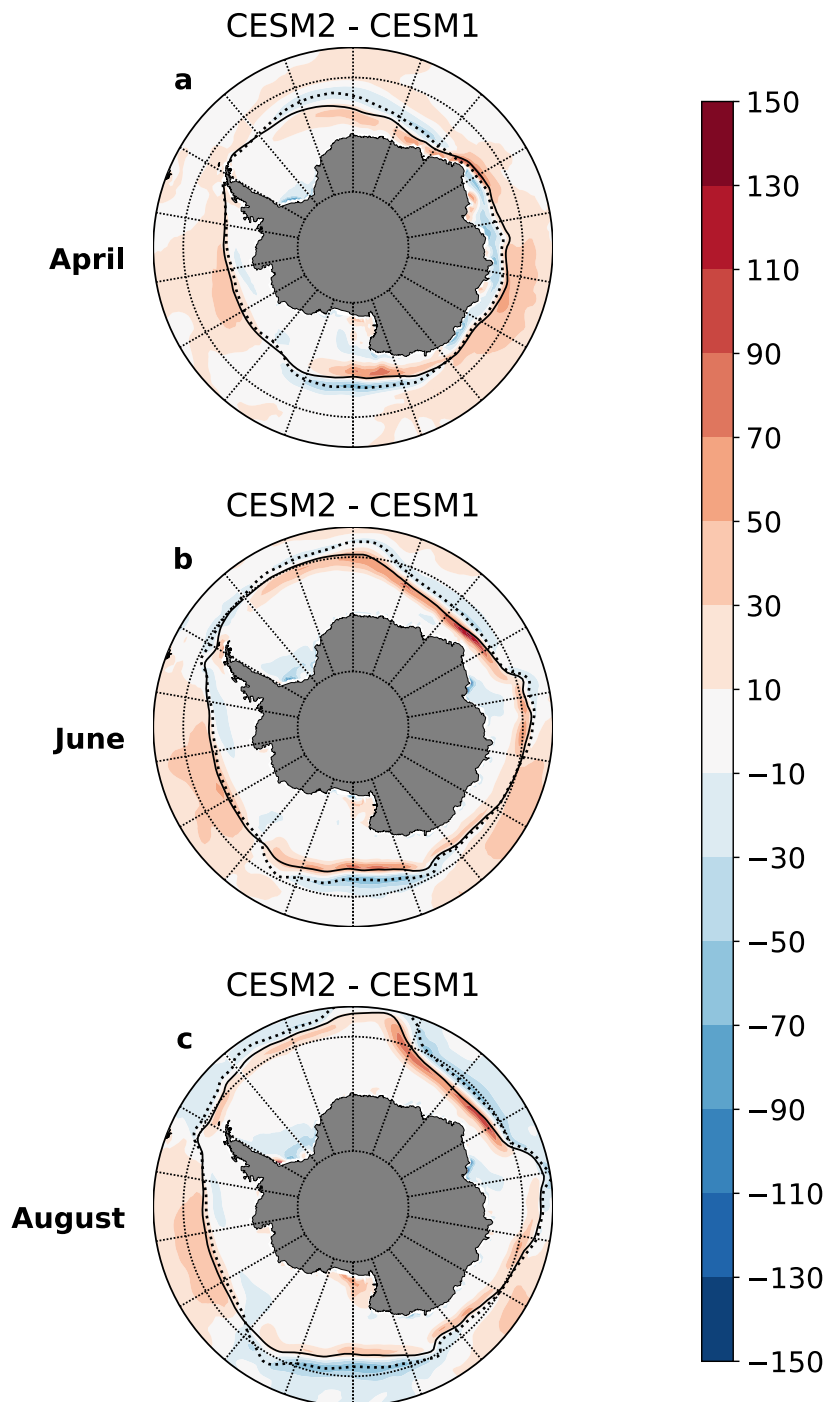


**Figure 16. Ocean Heat Flux Convergence during the Sea Ice Growth Season:** Difference between the monthly mean ocean heat flux convergence into the ocean mixed layer in CESM2 and CESM1 (in W/m<sup>2</sup>; colors) in (a) April, (b) June, and (c) August. Solid and dashed contours in each panel show the sea ice extent in CESM2 and CESM1, respectively.